Arabian Journal of Geosciences (2022) 15: 1313
https://doi.org/10.1007/s12517-022-10596-3

ORIGINAL PAPER

Main controlling factors and enrichment model of a multi-layer tight sandstone gas reservoir: case study from the Linxing Gas Field, eastern Ordos Basin, Northern China

Weitao Wu[1,2] · Jingzhou Zhao[1,2] · Yingbin Wang[3,4] · Mingqiang Guo[3,4] · Heyuan Wu[1,2] · Jun Li[1,2] · Jiacheng Dang[1,2]

Received: 14 March 2022 / Accepted: 3 July 2022 / Published online: 20 July 2022

Abstract
Determining the main controlling factors and the enrichment model of a tight sandstone gas (TSG) accumulation remains a key challenge in natural gas exploration. The characteristics and main controlling factors of a TSG reservoir were determined, and multi-part enrichment models were observed in the Linxing gas field. The main lithology of the gas-producing layers is medium- to coarse-grained lithic arkose sandstone with an average porosity of 10.11% and median permeability of 0.81×10^{-3} μm^2. The TSG reservoir comprises two sub-types: a lenticular lithological reservoir and a lithological-fault reservoir; these show vertically superimposed and laterally continuous quasi-continuous distribution. This enrichment of the multi-layer TSG is controlled by the reservoir, gas source, fault, and structural high point that respectively possesses distribution laws of "high-quality reservoir enrichment," "sufficient gas source supply," "moderate fault efficiency," and "favorable local high point." As the enrichment factors of natural gas are markedly different at various layers and areas, the enrichment models can be categorized into three groups that represent different areas: (1) X area: Excellent reservoir, highly efficient fault system, near-source gas-rich model; (2) Y area: Excellent reservoir, favorable high point, in- and adjacent-source gas-rich model; (3) Z area: Moderately good reservoir, over-developed fault system, gas-poor model, distributed around the Zijinshan Structural Belt. The findings of this study are expected to provide a theoretical basis for expanding the enrichment model theory of TSG and aid in locating TSG reservoirs in multi-layer exploration target settings.

Keywords Tight sandstone gas · Main controlling factors · Natural gas enrichment model · Linxing Gas Field · Ordos Basin

Introduction

With the continuous innovation of natural gas geological theory and a successive improvement of fracturing technology (Feng et al. 2019; Bou-Hamdan and Abbas 2021), tight sandstone gas (TSG) has become an important part of unconventional natural gas resources. The cumulative proven reserves and annual production of TSG in China are 5.2×10^{12} m^3 and 410×10^{8} m^3, respectively (as of 2019), only following that of the USA and Canada (Zou and Qiu 2021). Breakthroughs in the exploration of TSG have been made in the Tarim and Junggar basins in the west, the Ordos and Sichuan basins at the center, as well as the Songliao and Bohai Bay basins in the east of China, forming different levels and scales of TSG fields (Dai et al. 2019; Sun et al. 2019). Specifically, the TSG in the Upper Paleozoic sequences of the Ordos Basin is one of the most representative gas fields in the world (Fu et al. 2008; Yang et al. 2008, 2012; He et al. 2021; Wu et al. 2021b, 2022).

The TSG field group in the central Ordos Basin, comprising the Sulige, Wushenqi, Yulin, Zizhou, and Shenmu gas fields, was formed under favorable conditions described as "gentle tectonic setting, wide overlying hydrocarbon generation, large area sand body distribution, and stable tectonic activity" (Yang et al. 2012; Tang et al. 2012; Huang et al.

Responsible Editor: François Roure

✉ Weitao Wu
wtwu@xsyu.edu.cn

1 School of Earth Sciences and Engineering, Xi'an Shiyou University, Xi'an 710065, Shaanxi, China

2 Shaanxi Key Lab of Petroleum Accumulation Geology, Xi'an 710065, Shaanxi, China

3 Unconventional Oil and Gas Branch, CNOOC Ltd, Beijing 100016, China

4 China United Coalbed Methane Company Limited, Beijing 100016, China

2015; Zhao et al. 2017, 2019). However, TSG exploration in the Linxing area along the eastern margin of the Ordos Basin has progressed slowly because of the fact that the coalbed methane is still in its early stages of exploration (Chen et al. 2014; Li et al. 2014, 2016; Xie et al. 2016), and due to the influences of regional fault activity in the Zijinshan Structural Belt (Wang et al. 2007; Chen et al. 2012). With the intensification of TSG exploration and the deepening of gas geological theories, three core ideas have now been elucidated. (1) Coal-measure source rocks distributed from the Carboniferous Benxi Formation to the Permian Shanxi Formation are the main sources for controlling the formation and distribution of TSG (Fu et al. 2016; Xie et al. 2016; Li et al. 2016; Song et al. 2019; Xue et al. 2019; Hu et al. 2020; Zheng et al. 2020; Du et al. 2021; Shen et al. 2021); (2) Sandstone reservoirs mainly have nano-micron pores and are, hence, classified as tight reservoirs (Kong et al. 2020; Yin et al. 2020; Du et al. 2021; Jiu et al. 2021; Mi and Zhu 2021); (3) Activity within the Zijinshan Structural Belt controls hydrocarbon generation by the source rocks and the distribution of shallow gas reservoirs (Zou et al. 2016; Ge et al. 2018; Li et al. 2019a; Shu et al. 2019, 2021). These considerations have accelerated breakthroughs in TSG exploration and led to the discovery of TSG fields in the Linxing area with proven reserves of 1000×10^8 m^3 (Du et al. 2021).

The Linxing Gas Field (LGF) contains more than 10 layers of commercial gas flow, including the Carboniferous Benxi Formation, the Lower Permian Taiyuan and Shanxi formations, the Middle Permian Lower Shihezi and Upper Shihezi formations, and the Upper Permian Shiqianfeng Formation (Fu et al. 2016), compared with the TSG field group in the central Ordos Basin that contains concentrated gas-producing layers. The characteristics of multi-layer gas fields in the LGF are rare—not only in China, but also worldwide. According to the theory of gas migration and accumulation, the degree of gas filling in the trap and the yield will decrease with an increase in gas migration distance in the multiple-layer gas reservoirs. However, gas testing results showed that high yields can be obtained in the Upper and Lower Shihezi formations, which are at a greater distance from the source rocks than that of the Shanxi and Taiyuan formations. For example, the absolute open flow (AOF) of the second member (He6 Member) of the Lower Shihezi Formation is 17.7×10^8 m^3, whereas that of the fourth member (He4 Member) of the Upper Shihezi Formation can reach 32.6×10^8 m^3. Previous studies on LGF have mostly focused on reservoir-forming conditions or the controlling effect of a single formation condition (Chen et al. 2018; Ge et al. 2018; Song et al. 2019). Yet, studies on controlling factors and the enrichment model of multi-layer TSG accumulation have not been published. Therefore, this study delves into the main controlling factors of gas accumulation and establishes an enrichment model using seismic data, drilling, logging, gas testing, laboratory analysis, and other data as an example of multi-layer TSG at the LGF. The aim of this study is to enrich the accumulation theory of TSG and provide theoretical guidance for the discovery of multi-layer gas fields in similar basins.

Geological setting

The Ordos Basin, located in central China (Fig. 1a), is structurally divided into six first-order tectonic units (Fig. 1b), namely, the Yishan Slope, Tianhuan Depression, Western Thrust Belt, Jinxi Flexure Belt, Yimeng Uplift, and Weibei Uplift, with a total area of ~ 25×10^4 km^2. The LGF is in the Lin County–Xing County area, in western Shanxi Province. It structurally encompasses the transition between the Yishan Slope and the Jinxi Flexure Belt (Fig. 1b), covering an area of ~ 2000 km^2. This rock mass of the Zijinshan Structural Belt is in the southeast of the LGF (Fig. 1c), and it is mainly an alkaline or partially alkaline complex that consists of intrusive and extrusive rocks. Additionally, the rock mass of the Zijinshan Structural Belt has its top exposed at the surface (Huang 1991; Chen et al. 2012).

The structure in the middle and eastern part of Ordos Basin is an east dip monocline after the Caledonian uplift, which is a stable sedimentary stage until late Permian. Four uplift and denudation events have occurred since the Indosinian Movement, and the denudation thickness in the eastern part of the basin was the largest since Cretaceous (Chen et al. 2006; Li et al. 2019a), at over 1700 m (Fu et al. 2016), which formed the present west-dipping monocline. A series of intensive fault zones developed around the Zijinshan Structural Belt in the southeast part of the Linxing area owing to the uplift of rock mass in the Cretaceous, and a complex fault system related to regional stress was formed in the east (Ge et al. 2018). The structure of the Upper Paleozoic is characterized by good inheritance: high in the northeast and low in the southwest. For example, the top altitude of the He8 Member of the Lower Shihezi Formation gradually decreases from northeast to southwest, with a distribution range of − 600 to − 850 m (Fig. 1c), while local highs exist near the position of wells G5 and G6 (Fig. 1c). In the southeast, the maximum altitude can exceed − 350 m because of the uplift of the Zijinshan rocks mass. The stratum is composed of Cambrian and Ordovician sequences of the Lower Paleozoic; Carboniferous and Permian sequences of the Upper Paleozoic; Triassic, Jurassic, and Cretaceous sequences of the Mesozoic; and Quaternary sequences of the Cenozoic. A variety of lithologies were developed in the coastal barrier deposits of the Carboniferous Benxi and Permian Taiyuan formations, comprising primarily dark gray mudstone, micritic limestone, light gray medium sandstone, and thin coal seams. The fluvial delta system of regressive

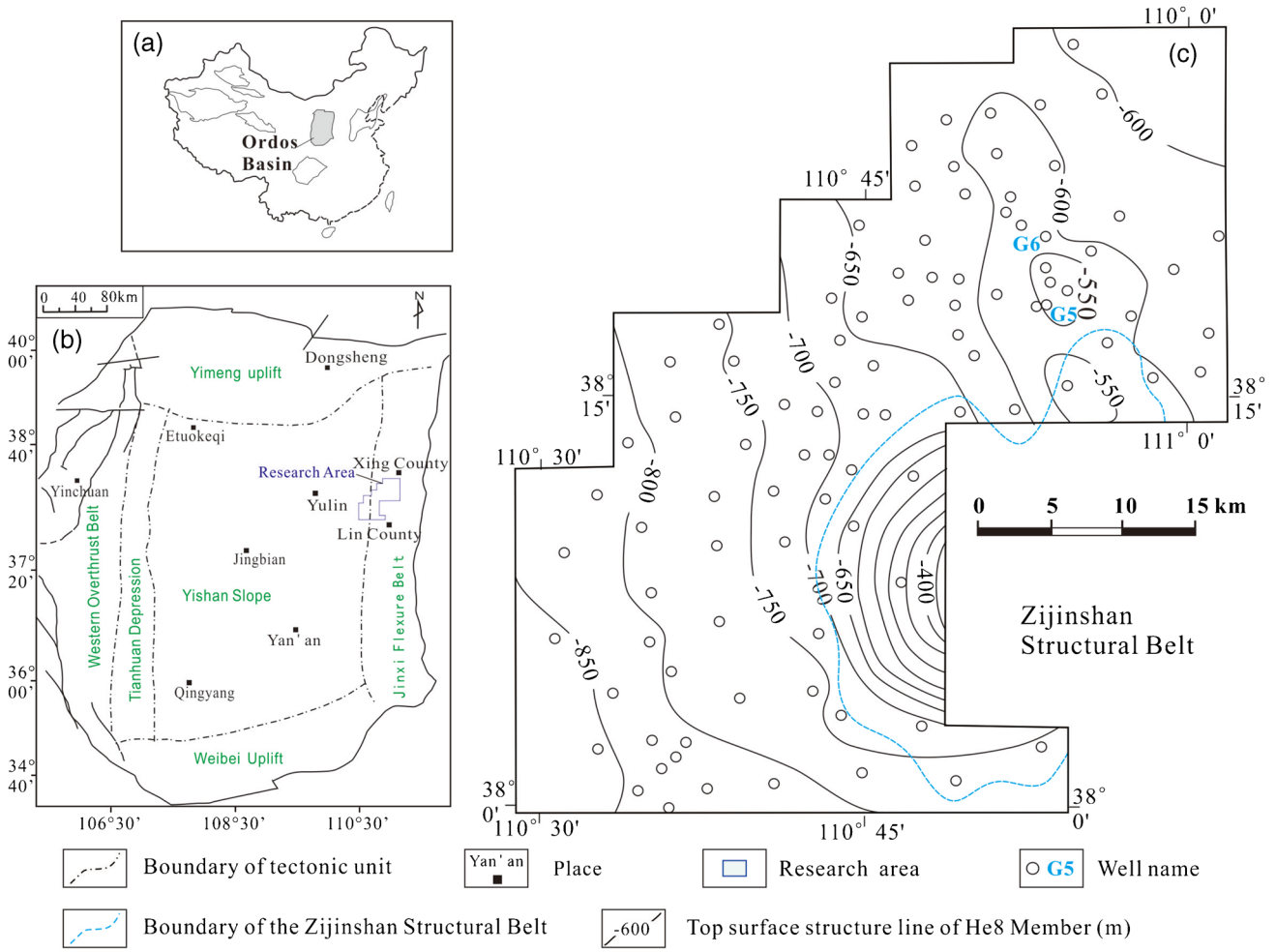

Fig. 1 Map of the Ordos Basin location; (**b**) map of the Linxing Gas Field (LGF) location; (**c**) structural map of the top surface of the He8 Member of the Permian Lower Shihezi Formation, which shows a trend of high in the northeast and low in the southwest

deposition is developed in the Shanxi Formation, which is dominated by medium-coarse sandstone, mudstone, and thin coal seam. The fluvial−deltaic facies occurred in the Permian Upper Shihezi, Lower Shihezi, and Shiqianfeng formations, with medium-coarse sandstone and gray mudstone (Fig. 2).

Database and methods

The data for this study comprises the following for Upper Paleozoic sequences of the LGF: gas testing results of 105 layers from 75 wells; reservoir porosity of 5661 samples and permeability of 5659 samples from 92 wells; gas components of 33 wells and gas isotopes of 14 wells; the content of total organic carbon (TOC) of coal seams from 29 samples and that of mudstone from 40 samples; hydrocarbon generating potential ($S_1 + S_2$) of coal seams from 25 samples and that of mudstone from 38 samples; vitrinite reflectance (R_o) of coal seams from 70 samples; and the pyrolysis peak temperature (T_{max}) from 57 samples. All data were provided by the Unconventional Oil and Gas Branch of China National Offshore Oil Corporation.

Calculation and measurement of reservoir parameters

In total, 30 plain and 30 casting thin sections were used to analyze the lithology and determine the reservoir space. Then, 80 samples were viewed using scanning electron microscopy (SEM) performed with a Quanta FEG 450 system at the Key Laboratory of Hydrocarbon Accumulation Geology of Shaanxi Province in Xi'an Shiyou University. The sand body showed typical well-logging characteristics of "three low and one high," i.e., low natural gamma (GR), low spontaneous potential (SP), low acoustic time difference (AC), and high resistivity (RT). We used a logging response to analyze and explain the sand body. Then, the average and

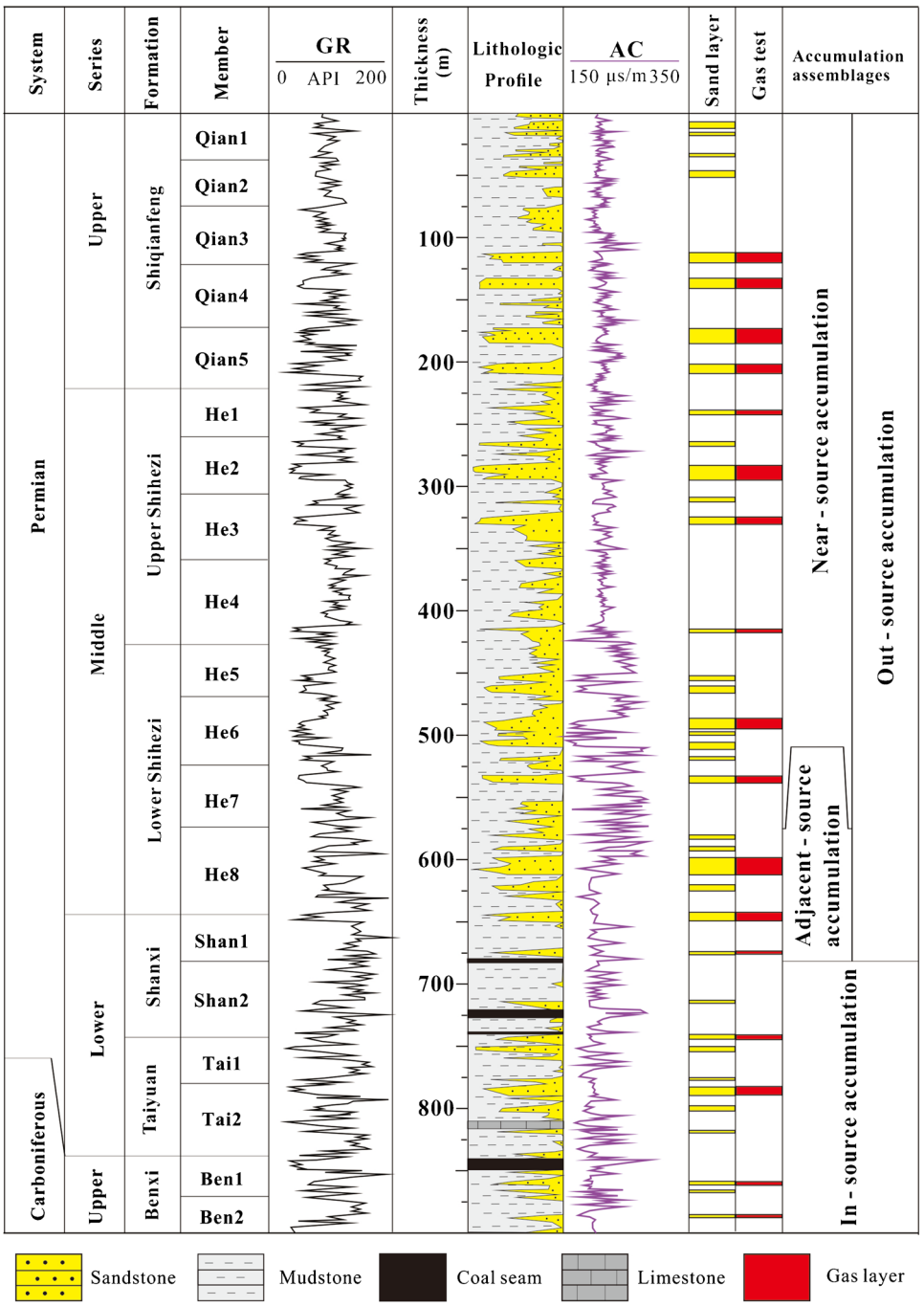

Fig. 2 Comprehensive lithostratigraphic profile of the Upper Paleozoic sequences in the LGF. The red segments represent the gas-producing layers, and the final column shows the source-reservoir accumulation assemblage

median values of porosity, permeability, thickness, and argillaceous content corresponding to the depth of the sand body were calculated (Table 1).

Calculation and measurement of source rock parameters

The thickness of the coal seams and dark mudstone were obtained from the cores of wells and their logging response. It was found that the logging features of the coal seam were characterized by high AC, high RT, low GR, high compensated neutrons (CNL), low density (DEN), and a low photoelectric absorption interface index (PE). The dark mudstone was characterized by high SP, high GR, and low AC. These response features were used to determine the thickness of the coal seams and mudstone of 97 wells.

The hydrocarbon generation intensity (*HGI*) of source rocks is a comprehensive index to evaluate their hydrocarbon generation ability. The HGI was calculated using the following formula:

Table 1 Statistics of formation condition parameters of TSG reservoirs in the LGF

Well	Member	Top depth (m)	Bottom depth (m)	Bushing elevation (m)	AOF ($10^4m^3/d$)	Coal seam thickness (m)	HGI ($10^8m^3/km^2$)	Φ (%)	K ($10^{-3}\mu m^2$)	V_{sh} (%)	Distance (km)
B1	He8	1641.8	1651.9	1025.6	0.85	31.0	44.9	7.0	0.24	12.0	2.68
B1	Qian5	1279.2	1288.5	1025.6	0.56	31.0	44.9	10.5	1.89	12.1	2.68
B1	He4	1466.5	1472.1	1025.6	3.10	31.0	44.9	8.6	1.69	16.8	2.68
B2	He6	1660.7	1666.1	1131.5	2.00	16.6	26.7			10.2	0.93
G1	Ben1	2059.3	2066.1	1008.0	4.79	14.4	23.8	9.9	4.95	11.4	3.73
G2	Tai1	1866.5	1875.3	945.1	0.53	13.9	17.2	8.8	0.10	27.9	1.89
G3	He2	1458.4	1466.8	1048.9	17.30	23.4	24	14.4	14.40	4.9	1.99
G3	He4	1590.4	1593.9	1048.9	16.20	23.4	24	12.9	32.10	6.3	1.99
G4	He7	1514.8	1519.2	941.8	1.21	22.1	15.6	6.6	0.15	8.9	1.02
G4	He6	1473.2	1480.1	941.8	1.83	22.1	15.6	10.1	1.01	10.7	1.02
G5	He8	1567.5	1571.6	1012.7	2.85	22.7	18.6	6.6	5.50	8.2	0.66
G5	Tai2	1790.7	1803.7	1012.7	13.27	22.7	18.6	8.6	1.38	10.3	0.66
G5	He7	1549.3	1553.1	1012.7	6.18	22.7	18.6	13.0	4.15	18.2	0.66
G6	He8	1485.4	1491.4	928.6	0.29	19.7	20.3	5.4	0.40	22.1	1.27
G6	Tai2	1702.2	1715.0	828.6	0.50	19.7	20.3	9.7	0.60	19.8	1.27
G6	He6	1437.1	1441.5	928.6	0.10	19.7	20.3			30.1	1.27
G7	He2	1377.5	1381.5	1060.0	0.84	23.0	17.3			11.4	0.89
G7	Qian4	1260.8	1264.8	1060.0	0.36	23.0	17.3			10.5	0.89
G7	Qian5	1312.8	1320.0	1060.0	0.36	23.0	17.3			18.3	0.89
G8	He2	1398.5	1402.5	1022.2	3.45	19.4	17.2	12.0	0.83	10.2	1.73
G8	He2	1363.0	1367.0	1022.2	3.45	19.4	17.2	9.6	0.48	11.3	1.73
H3	He6	1674.8	1685.5	1050.4	7.58	24	22.7	12.6	1.02	11.7	2.27
H3	He7	1709.4	1715.5	1050.4	7.58	24	22.7	12.1	1.48	14.4	2.27
H4	He3	1599.3	1606.8	1120.9	1.94	24.4	17.9			12.4	3.21
H6	He6	1684.5	1693.3	1063.3	5.68	22.2	20.1	11.9	1.49	10.0	1.43
H7	He6	1635.2	1642.3	1001.5	4.50	11.5	16.8	9.3	1.08	4.7	1.74
Q1	Qian4	1266.6	1269.6	1005.1	0.35	19.7	19.7	11.9	1.05	6.8	1.43
Q1	He6	1558.0	1561.0	1005.1	0.35	19.7	19.7	9.5	0.41	7.2	1.43
Q10	He4	1440.9	1446.9	959.6	3.31	19.1	13.7	12.9	3.09	11.9	0.91
Q10	Qian5	1244.6	1248.4	959.6	0.65	19.1	13.7	10.1	2.83	17.0	0.91
Q11	Qian4	1064.9	1071.2	828.3	1.98	15.6	16.1	11.0	5.64	15.9	0.98
Q11	He7	1477.5	1505.2	828.3	0.90	15.6	16.1	13.3	5.70	21.5	0.98
Q11	He1	1203.8	1211.9	828.3	0.62	15.6	16.1	9.1	8.50	22.8	0.98
Q12	He4	1343.7	1363.5	864.4	2.20	15.2	12.6			5.9	0.56

Table 1 (continued)

Well	Member	Top depth (m)	Bottom depth (m)	Bushing elevation (m)	AOF ($10^4m^3/d$)	Coal seam thickness (m)	HGI ($10^8m^3/km^2$)	Φ (%)	K ($10^{-3}\mu m^2$)	V_{sh} (%)	Distance (km)
Q13	He3	1456.8	1459.5	1087.2	0.89	19.2	15.4	5.7	0.32	16.4	0.58
Q14	He4	1348.3	1356.6	914.1	5.06	26.7	33.9	9.2	0.33	13.3	1.06
Q15	He1	1169.0	1179.9	936.8	4.04	20.7	18.4			12.6	1.54
Q15	He4	1316.6	1322.5	936.8	7.68	20.7	18.4			18.5	1.54
Q16	Tai2	1726.4	1733.3	958.8	9.64	26.0	18.2	8.9	1.15	6.7	1.28
Q16	He3	1291.5	1295.9	958.8	1.34	26.0	18.2	7.8	1.07	13.5	1.28
Q17	He8	1597.5	1615.0	1060.2	0.94	15.6	19.1			14.4	1.15
Q17	Shan1	1689.5	1696.9	1060.2	0.24	15.6	19.1			23.5	1.15
Q18	He8	1562.5	1586.2	972.0	0.97	16.7	28.5			16.2	1.73
Q19	He8	1771.3	1776.3	1171.4	0.47	17.0	12.3	10.7	0.86	20.5	1.02
Q2	He7	1838.8	1842.8	1375.4	0.51	26.4	21.3			10.8	6.1
Q3	He3	1447.5	1451.5	1020.8	8.94	16.1	14.6			5.8	5.9
Q4	He8	1650.0	1654.0	985.3	0.37	20.6	17.3	9.2	0.07	13.0	4.1
Q4	He7	1638.0	1640.0	985.3	0.37	20.6	17.3	9.4	0.17	17.2	4.1
Q4	He2	1372.5	1378.0	985.3	1.01	20.6	17.3			10.5	4.1
Q5	He2	1188.8	1191.8	801.4	0.98	12.7	12.2			11.4	1.98
Q5	He6	1408.8	1411.8	801.4	1.26	12.7	12.2			9.8	1.98
Q5	He7	1449.6	1452.6	801.4	1.26	12.7	12.2			19.6	1.98
Q6	He2	1308.0	1311.0	1006.9	6.18	22.2	16.6	7.9	3.24	8.3	0.84
Q6	He2	1321.5	1324.5	1006.9	6.18	22.2	16.6	9.7	1.50	8.5	2.12
Q6	He2	1363.5	1366.5	1006.9	6.18	22.2	16.6	10.0	1.48	10.3	0.84
Q6	He3	1424.0	1428.0	1006.9	6.18	22.2	16.6			10.6	0.84
Q7	He2	1418.0	1420.0	1100.4	7.48	21.76	18.9	13.0	11.00	7.0	1.59
Q7	He7	1669.5	1671.5	1100.4	1.79	21.8	18.9	14.8	0.50	9.1	1.14
Q7	He2	1396.0	1398.5	1100.4	7.48	21.8	18.9	12.6	0.55	9.7	1.59
Q8	He2	1442.0	1445.0	1125.4	0.56	11.5	12	13.1	1.25	7.2	1.27
Q9	He7	1557.5	1560.5	1037.6	0.77	23	22.9	10.2	0.59	8.5	1.59
Q9	He2	1303.0	1307.0	1037.6	1.00	23	22.9	11.5	0.70	9.3	1.59
Q9	Shan2	1730.0	1740.0	1037.6	0.03	23	22.9	7.9	0.17	10.0	1.59
Q9	He7	1579.5	1582.5	1037.6	0.77	23	22.9	9.1	0.37	10.1	1.59
W1	Tai2	1992.3	1999.5	1172.8	0.03	19.2	32.1	7.6	0.76	29.4	0.29
W10	He2	1592.1	1599.0	1022.5	3.50	13.8	19.4	12.6	12.40	5.2	2.12
W11	Shan2	1933.8	1938.8	985.9	2.03	21.5	25.1	6.7	0.10	10.9	1.16
W12	He6	1784.0	1788.8	973.7	1.56	17.9	28.5			8.9	2.35

Table 1 (continued)

Well	Member	Top depth (m)	Bottom depth (m)	Bushing elevation (m)	AOF ($10^4m^3/d$)	Coal seam thickness (m)	HGI ($10^8m^3/km^2$)	Φ (%)	K ($10^{-3}\mu m^2$)	V_{sh} (%)	Distance (km)
W13	He8	1704.6	1713.3	953.0	0.67	15.4	37.1	8.3	0.80	12.9	0.70
W14	He2	1589.0	1595.9	1038.6	1.24	18.3	33.6			9.1	1.12
W15	Qian4	1680.0	1684.0	860.8	1.12	19.6	35.2			7.4	3.24
W16	Tai2	1933.1	1945.7	956.8	7.30	12.7	18.1	12.1	0.43	6.5	1.49
W17	Tai2	1982.5	1996.7	985.9	1.79	12.5	18.8	9.2	0.11	17.2	1.73
W18	He4	1569.1	1573.0	1064.6	32.60	17.5	14.6	15.9	11.10	3.5	1.15
W18	He2	1610.0	1614.6	958.6	1.04	24.5	32.3	12.2	6.79	12.3	4.98
W18	Qian5	1527.0	1532.0	958.6	1.95	24.5	32.3			4.9	2.1
W2	Tai1	1893.5	1904.8	1111.7	0.24	25.5	39.8	7.6	0.29	18.8	0.53
W3	He8	1817.4	1839.6	1144.6	0.97	12.9	17.4	7.2	0.18	24.3	1.18
W4	Tai2	2061.4	2064.5	1089.5	2.85	15.3	30.2	8.4	0.49	22.0	5.79
W5	He8	1926.4	1931.8	1111.6	1.48	18.5	25.3	13.3	0.67	6.6	1.59
W6	He7	1739.2	1748.0	947.5	0.68	15.8	24.9			12.1	2.31
W7	He8	1883.0	1891.0	1039.0	0.36	14.1	24.4	7.7	1.57	19.4	3.1
W8	He2	1596.5	1598.7	1005.0	2.50	26.6	36.8	8.2	0.50	5.1	1.04
W8	He2	1601.0	1603.8	1005.0	2.50	26.6	36.8	12.1	0.25	6.6	1.04
W8	Ben1	2074.7	2080.5	1005.0	0.47	26.6	36.8	7.1	0.13	7.5	1.04
W9	He7	1863.7	1866.7	1043.6	14.60	14.8	21.5	12.8	0.27	4.6	1.20
W9	He7	1845.6	1851.3	1043.6	14.60	14.8	21.5	10.4	0.28	6.5	1.20

Note: Top depth and bottom depth are the depth of perforation interval

"Distance" refers to the distance between fault and well point

AOF absolute open flow, *HGI* hydrocarbon generation intensity, V_{sh} argillaceous content of gas sandstone obtained by logging

$$G_{gas} = H \times \rho_{rock} \times TOC \times K_g \times 10^{-3} \quad (1)$$

where, G_{gas} is the HGI of the source rock, $\times 10^8$ m^3/km^2; H is the coal seams and dark mudstone thickness of the source rock, m; ρ_{rock} is the density of the source rock, t/km^3 (in this study, the coal seam density was 1300 t/km^3, and dark mudstone density was 2600 t/km^3); TOC is the total content of organic carbon in the source rock, %; and K_{gas} is the gaseous hydrocarbon rate of the source rock, m^3/t·TOC.

Of the variables, ρ_{rock} was obtained from the logging curve, while the total content of organic carbon (TOC) was determined via mapping; K_{gas} was obtained from the thermal compression simulation test of coal seams and dark mudstone (Table 2) (Yang et al. 2016; Gao et al. 2018).

Results and discussion

Distribution and characteristics of the multi-layer TSG reservoir

Distribution of natural gas

Gas-producing wells were mainly concentrated in the north-central and southwestern parts of the LGF, with fewer wells near the Zijinshan Structural Belt, according to the gas test results (Fig. 3). Moreover, the number of gas-producing wells and AOFs were significantly different across sequences (Fig. 4). A total of 14 gas-producing layers were identified in sequence: the first member (Ben1 Member) of the Carboniferous Benxi Formation; the second (Tai2 Member) and first (Tai1 Member) members of the Lower Permian Taiyuan Formation; the second (Shan2 Member) and first (Shan1 Member) members of the Shanxi Formation; the fourth (He8 Member), third (He7 Member), and second (He6 Member) members of the Lower Shihezi Formation; the fourth (He4 Member), third (He3 Member), second (He2 Member), and first (He1 Member) members of the Upper Shihezi Formation; and the fifth (Qian5 Member) and fourth (Qian4 Member) members of the Shiqianfeng Formation. The number of producing layers and AOFs of the He2, He4, He6, He7, He8, and Tai2 members was greater than those of other layers. Within these members, there were 16 gas-producing layers in the He2 Member, with a maximum AOF of 16.2×10^4 m^3/d. The number of gas layers in the He4, He6, He7, He8, and Tai2 members was 8, 11, 11, 19, and 13, respectively, with maximum AOFs of 32.6×10^4, 7.58×10^4, 14.6×10^4, 6.18×10^4, and 13.3×10^4 m^3/d, respectively.

Reservoir conditions

The lithology of the gas reservoir was mainly lithic arkose, accounting for 55.4% of the total samples ($N = 325$), followed by arkosic lithic sandstone, while lithic sandstone and arkose was less than 10%. The lithologic grain size was mainly medium-coarse sandstone, followed by medium-fine sandstone, and a small amount of fine sandstone and silty sandstone. The reservoir space mainly consisted of remanent intergranular pores, inter- and intragranular dissolution pores, followed by inter-crystalline and micro-fissure pores.

Based on the analysis of reservoir physical properties, the porosity ranged from 0.3 to 23.5% ($N = 5661$), with an average of 7.89% and a median of 7.61%, and samples that had less than 10% porosity accounted for 74.9% of the total. The permeability ranged from 0.01×10^{-3} to 549.1×10^{-3} μm^2 ($N = 5659$), with an average of 2.86×10^{-3} μm^2 and a median of 0.43×10^{-3} μm^2. Furthermore, 77.7% of the samples had permeability less than 1×10^{-3} μm^2. Therefore, the reservoir type could be categorized as low porosity and low permeability. In terms of the horizon (Fig. 5), the physical properties of the He4 Member were most favorable, followed by the Qian5, He2, He6, and Tai2 members. Among them, the He4 Member had the highest porosity (11.36%), followed by He2 and He6 members (both over 9.3%), and Shan1 and Shan2 members had the lowest porosity (both less than 6%). The median permeability of He4 Member was the highest, reaching 1.59×10^{-3} μm^2, followed by Qian5, He2, and Tai2 members, which were greater than 0.5×10^{-3} μm^2, and the permeability of the other layers were all less than 0.1×10^{-3} μm^2. The average permeability of the Qian5 Member was the highest, at more than 10×10^{-3} μm^2, while that of the He2 and He4 members was higher than 6×10^{-3} μm^2, and that of the Qian1, Qian2, Qian3, Shan1, and Tai1 members less than 0.2×10^{-3} μm^2.

Overall, the gas reservoir in the Upper Paleozoic strata of the LGF belonged to a TSG reservoir. According to the physical property statistics of the gas-producing sand body ($N = 63$) (Fig. 6), the porosity ranged from 5.38 to 15.89%,

Table 2 Hydrocarbon production rate (K_{gas}) of coal-measure source rocks with different lithologies in the Ordos Basin

R_o (%)	1	1.25	1.5	1.75	2	2.25	2.5
K_{gas} of coal seam in the second member of Shanxi Formation (Shan2 Member) (kg/t$_{TOC}$) (Yang et al. 2016)	23.2	66.5	80.5	91.2	102.5	111.6	120.5
K_{gas} of coal seam from Benxi Fm. to Taiyuan Formation (kg/t$_{TOC}$) (Yang et al. 2016)	20.5	39.6	44.9	49.1	52.1	55.6	57.6
K_{gas} of mudstone from Benxi Formation to Shan2 Member (kg/t$_{TOC}$) (Gao et al. 2018)	11.5	23.1	33.9	47.8	57.6	64.8	71.9

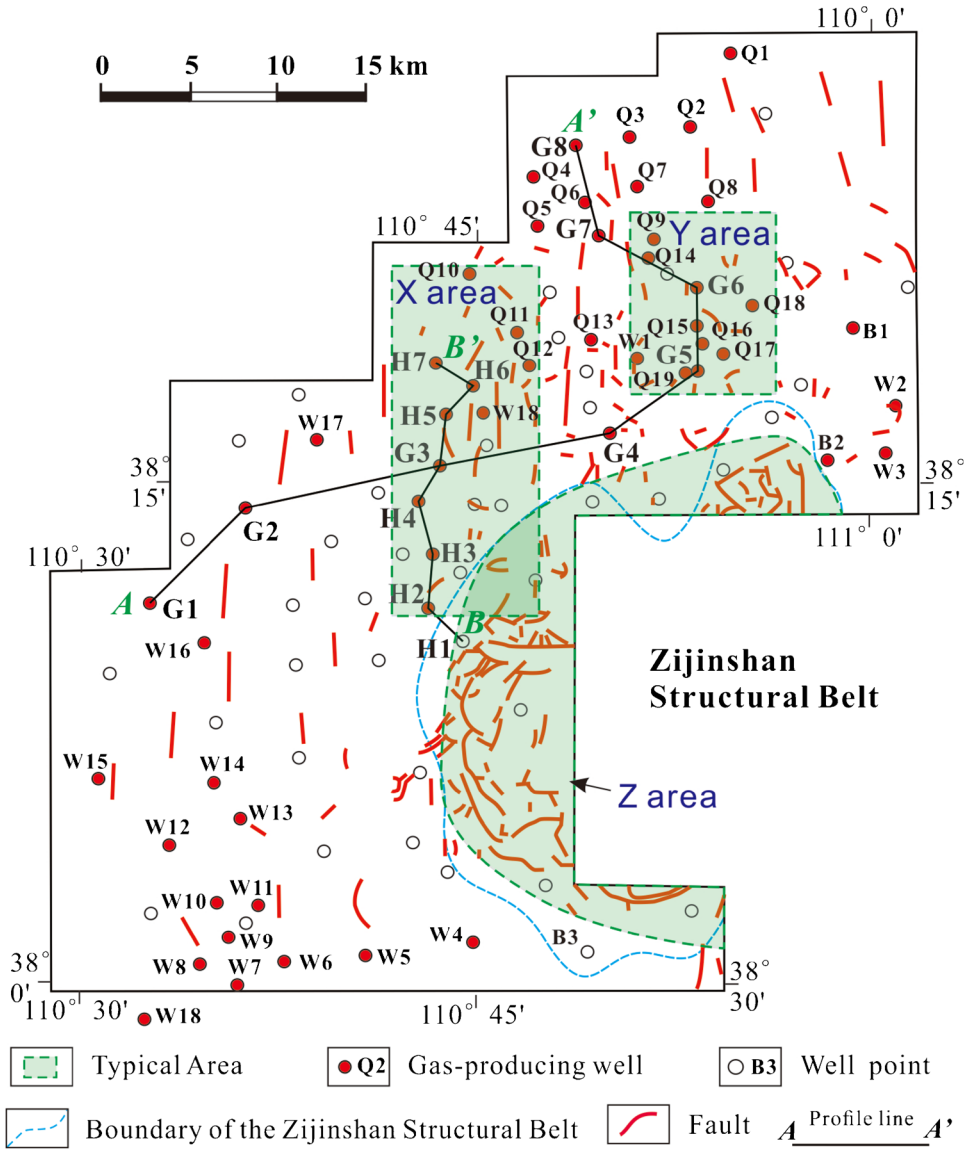

Fig. 3 Plan view of the fault development and wells in the Upper Paleozoic strata of the LGF. The red well points are gas-producing wells, the hollow points are non-gas-producing wells, and the blue dashed line is the boundary of the Zijinshan Structural Belt. The green-shaded X, Y, and Z areas are typical areas used to explain different gas enrichment model. The black lines with green text indicate the profile line positions, where A−A′ is shown in Fig. 7, and B−B′ is shown in Fig. 8

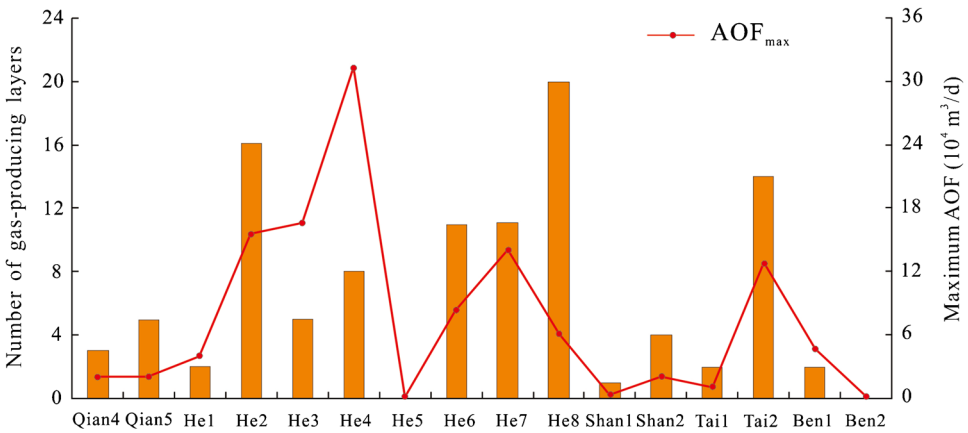

Fig. 4 Histogram of the number of gas-producing layers and maximum AOF in the LGF. The orange columns indicate the number of gas-producing layers according to the left ordinate, and the red line illustrates the maximum AOF values according to the right ordinate

with an average of 10.11%, and the permeability ranged from (0.07 to 32.1)$\times 10^{-3}$ μm^2, with an average of 2.61$\times 10^{-3}$ μm^2 and median of 0.81$\times 10^{-3}$ μm^2. For a single horizon, the average porosity and permeability of the Shiqianfeng

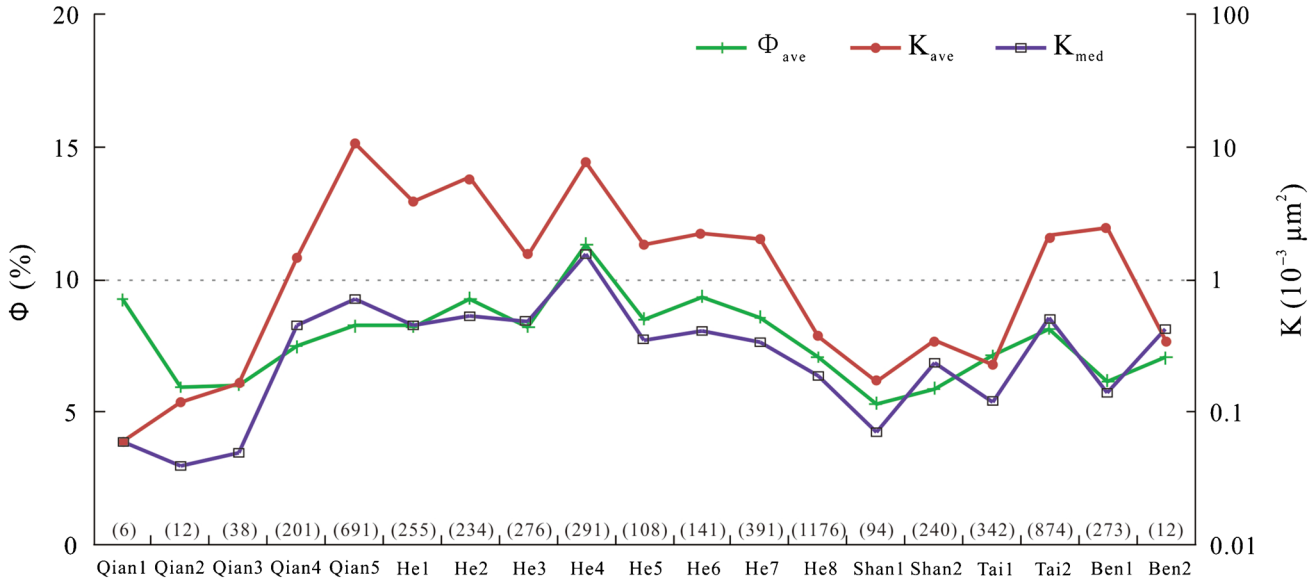

Fig. 5 Line map of reservoir physical properties in the LGF. The green line is the average porosity, the red line is the average permeability, and the purple line is the median permeability. The numbers in brackets at the bottom indicate the number of samples. The left ordinate is porosity, and the right ordinate is permeability

Formation ranged from 10 to 12% and $(1–10)\times10^{-3}$ μm^2, respectively, while those of the Upper Shihezi and Lower Shihezi formations varied widely, ranging from 4.5 to 16% and $(0.1–12)\times10^{-3}$ μm^2, respectively; and those of the Shanxi and Benxi formations were less than 10% and 1×10^{-3} μm^2, respectively. The porosity of gas reservoirs was positively correlated with permeability, i.e., the permeability increased gradually as porosity increased.

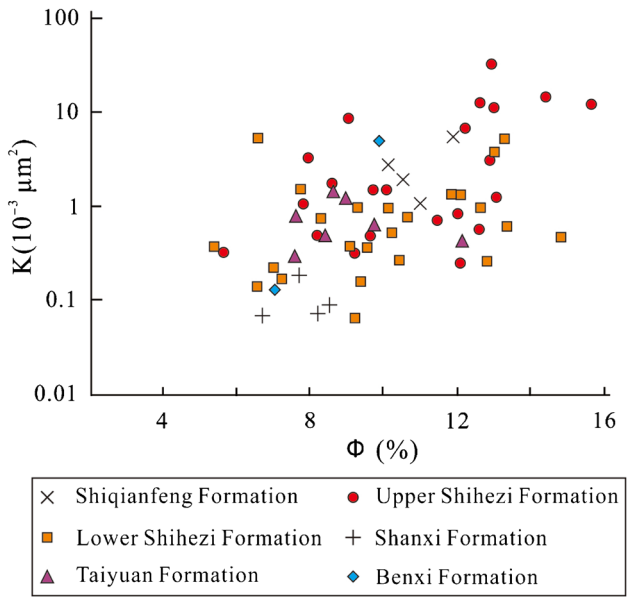

Fig. 6 Cross-plot of porosity vs. permeability of the gas reservoir in the LGF

Characteristics of the gas reservoir

Intertidal and distributary channel lenses were the main sandstone types of the gas reservoirs in the LGF developed in the Late Carboniferous–Early Permian barrier coast and tidal flat facies, as well as in the Middle–Late Permian fluvial-delta facies in the eastern margin of the Ordos Basin (Fu et al. 2008; Li et al. 2021). The multi-stage sand bodies were frequently transversely migrated, vertically superimposed, and continuously extended for hundreds of kilometers. Based on 525 logging interpretations of a single gas-bearing sandstone from 52 wells, the thickness ranged from 0.5 to 26.3 m with an average of 4.85 m, and 59.8% of the main body thickness ranged from 2 to 6 m. Among them, the thickness of the Qian5 Member was the largest—up to 10.5 m—followed by the He8 and Tai2 members with thickness 8.4 and 7.5 m, respectively, and the He2 and He4 members with 6.5 and 6.1 m, respectively. The Ben2 and Qian1 members had the smallest thickness—less than 2.5 m.

Fine-grained sedimentary rocks such as mudstone, argillaceous siltstone, and micritic limestone in different sedimentary facies from Benxi to Shiqianfeng formations were characterized by low porosity and permeability, small pore size, and high capillary pressure, with the mudstone dividing the sandstones into multi-layer lenses and sealing the sandstone. Regional geological evolution and seismic profiles show that the displacement of most of the fault developed in the Upper Paleozoic sequences between 5 and 15 m, which was larger than the thickness of the sandstone and played a sealing role. Therefore, lenticular lithologic traps

and fault-lithologic traps form the TSG reservoir groups, which were superposed vertically and continuously distributed horizontally (Figs. 7–8), presenting quasi-continuous distribution (Zhao et al. 2019; Wu et al. 2022). The TSG reservoir had no apparent edge or bottom water, and its formation water was mostly distributed in isolated lenses (Fig. 7). According to the gas testing results of exploration wells ($N=75$), 11 water-producing layers were distributed in Ben1, Ben2, Tai1, Tai2, Shan2, Shan1, He8, He4, He2, and Qian5 members, and their water yield was between 0.25 and 32.5 m^3, most of which were less than 4 m^3. In addition, there is poor connectivity between formation water.

Natural gas properties

The gas reservoir can be described as a dry gas reservoir. Based on the analysis of natural gas components and composition, the methane content ranged from 90.72 to 99.63% ($N=33$), with an average of 94.97%, and a methane content between 93 and 97% accounting for 57.5% of total number (Fig. 9a). The dryness coefficient ($C_1/\sum C$) ranged from 0.924 to 0.999, with an average of 0.974. The proportion of non-hydrocarbon components varied from 0.17 to 7.51% ($N=33$), and the maximum value of N_2 was 7.51%, which is related to air mixing in the sampling process. The $\delta^{13}C_1$ values ranged from −41.3 to −32.8‰ ($N=14$), with an average of −37.8‰, and the $\delta^{13}C_2$ values ranged from −28.9 to −22.3‰ ($N=11$), with an average of −26.3‰. Based on the gas identification diagram (Dai et al. 2014), the natural gas in the study area was from the coal-measure source rocks of the Benxi and Taiyuan formations, as well as the Shan2 Member of the Shanxi Formation.

Main controlling factors of multi-layer TSG accumulation

Controlling effects of the reservoir conditions

Physical properties The formation and enrichment of the TSG reservoir were notably controlled by the physical properties of the gas-producing sandstone. Based on the relationship of the sandstone physical properties and the AOF values of the gas test (Fig. 10a–b), the AOF value had a clear positive correlation with the reservoir porosity and permeability, i.e., it increased with increasing gas porosity or permeability. Furthermore, the AOF generally showed an upward trend. Permeability was more controlled than the porosity. Concerning each formation, with an increase in porosity, the AOF of the Upper Shihezi Formation increased notably, and

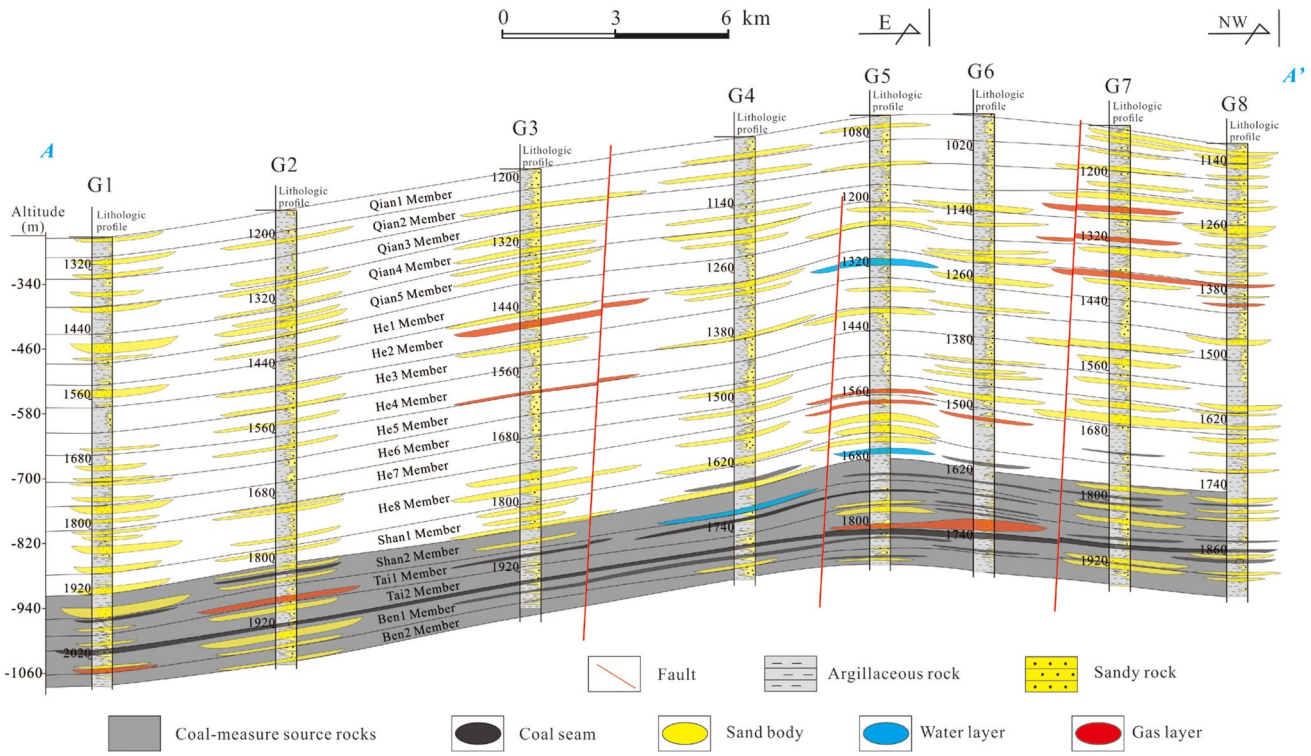

Fig. 7 Profile A–A′ of the gas reservoir distributed from Benxi and Shiqianfeng formations of the LGF. Yellow is sandstone, red is the gas-producing layer, blue is the water-producing layer, and black is the coal seam layer. The dark gray is the source rock location, and light gray is the argillaceous content in the lithologic profiles. The location of the profile is shown in Fig. 3

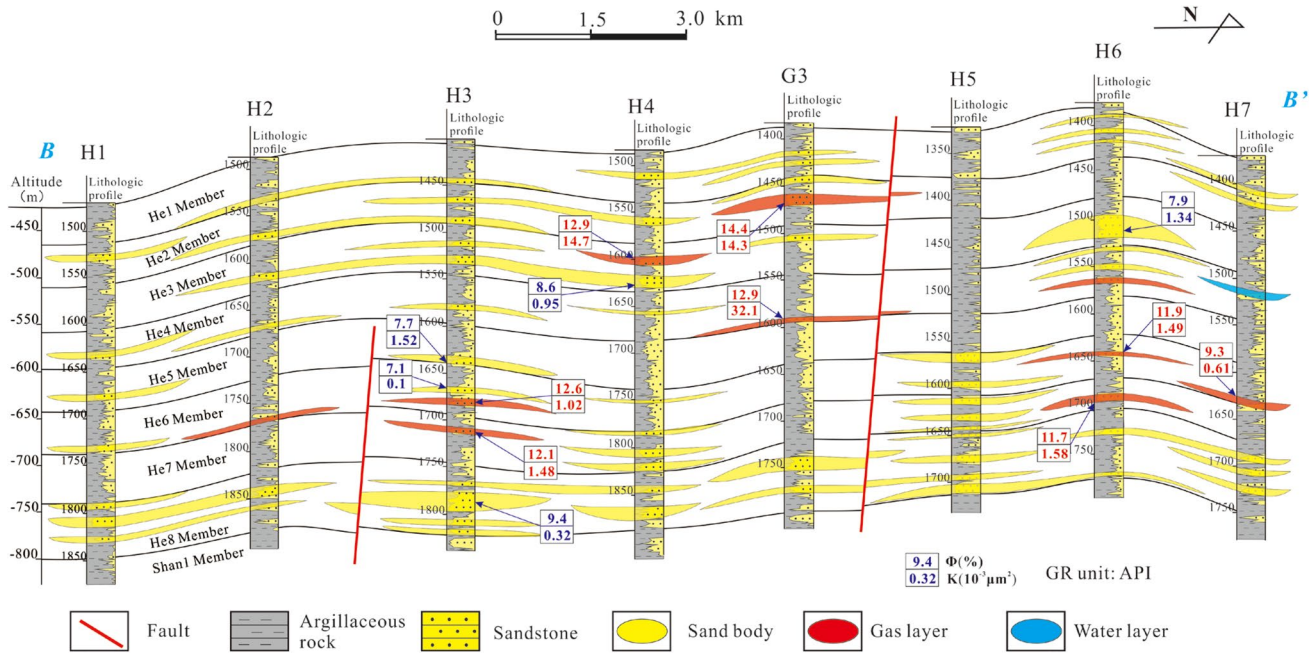

Fig. 8 Profile B−B′ of the gas reservoir distributed in the Lower Shihezi and Upper Shihezi formations of the LGF. Yellow is the sandstone layer, red is the gas-producing layer, and blue is the water-producing layer. Gray indicates the argillaceous content in the lithologic profile. The red numbers in the boxes are the porosity (top) and permeability (bottom) of the gas-producing layers, while the purple numbers are the porosity (top) and permeability (bottom) of the sandstone layers. The location of the profile is shown in Fig. 3

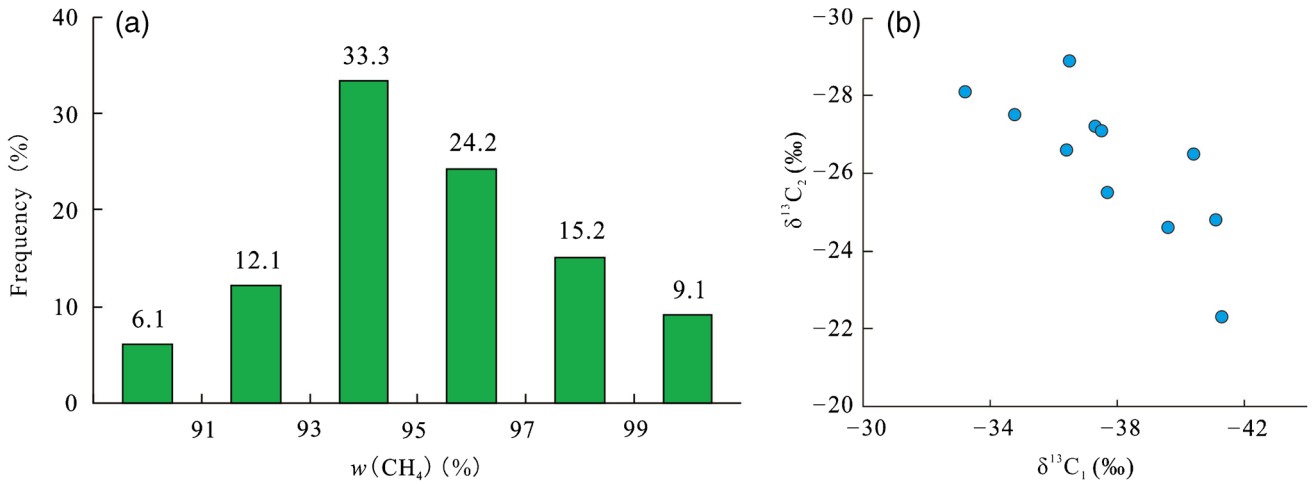

Fig. 9 Distribution of methane content and carbon isotope of natural gas in the Upper Paleozoic in Linxing gas field, Ordos basin. (**a**) Histogram of methane content. (**b**) Cross-plot of $\delta^{13}C_1$ vs. $\delta.^{13}C_2$

the AOF of the Lower Shihezi Formation also increased to a certain extent, while Taiyuan, Shanxi, and Shiqianfeng formations did not show an increasing trend, and the trend of the Benxi Formation was restricted by the number of data points. With increasing gas permeability, there was an apparent increase in AOF of the Upper Shihezi, Lower Shihezi, Shiqianfeng, and Taiyuan formations, and that of the Shanxi Formation essentially remained unchanged. From the gas reservoir profile of the wells H1–H7 (Fig. 8), the porosity and permeability of the gas-producing layer in each well were better than that of the unaerated sandstone layers. For example, the AOF of the He6 and He7 members in Well H3 was 6.18×10^4 m^3/d, the porosity of the reservoirs 12.6 and 12.1%, and the permeability 1.02×10^{-3} and 1.48×10^{-3} μm^2, which were significantly higher than the

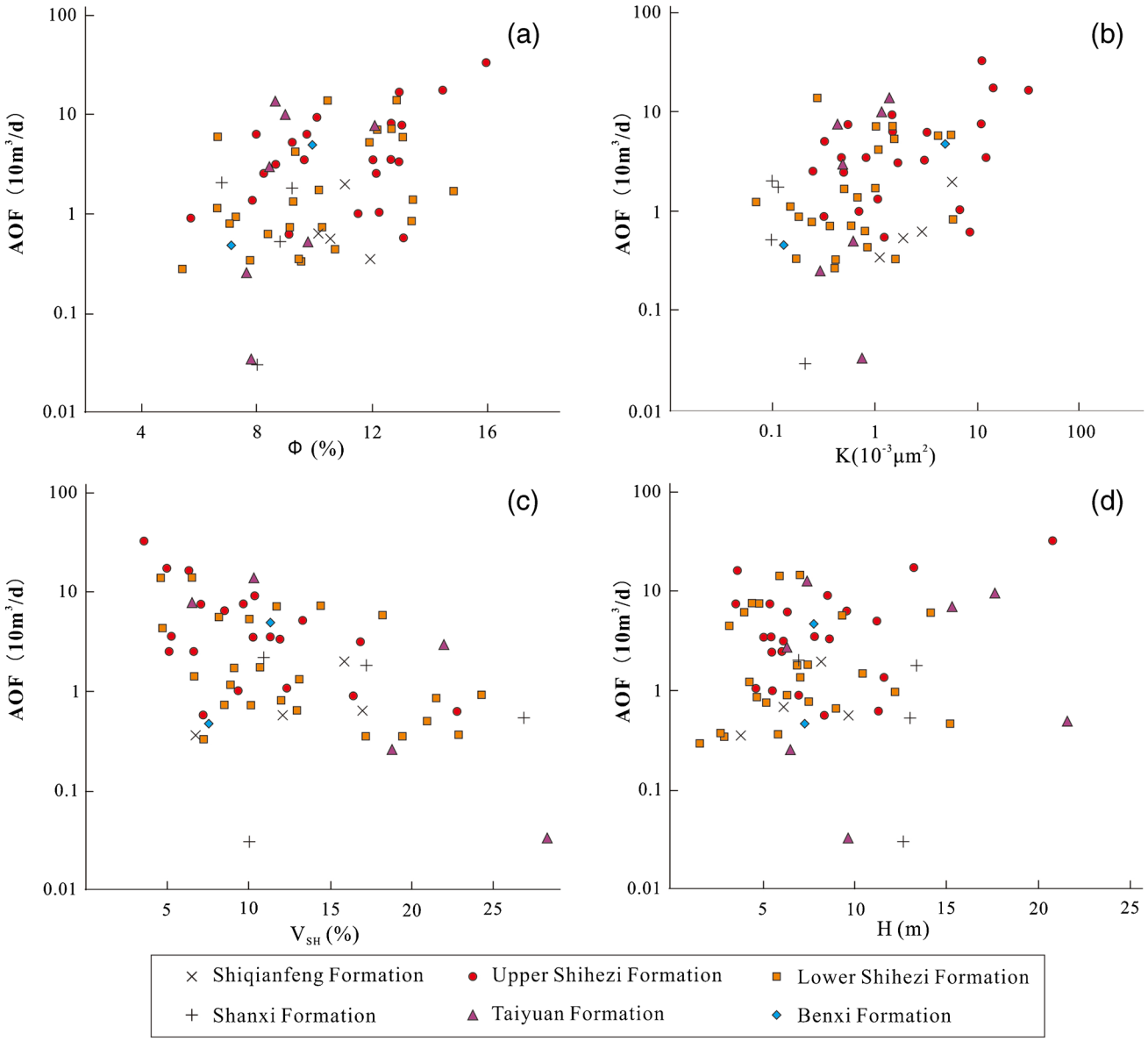

Fig. 10 Cross-plots of reservoir parameters and absolute open flow (AOF) in gas reservoir of the LGF. (**a**) Porosity (Φ) vs. AOF. (**b**) Permeability (K) vs. AOF. (**c**) Argillaceous content (V_{sh}) vs. AOF. (**d**) Sandstone thickness (H) vs. AOF

same properties of their adjacent reservoirs. Wells H4 and H6 also had similar characteristics.

Argillaceous content The AOF was noticeably controlled by the argillaceous content of the gas-producing sandstone. Argillaceous content ranged from 3.2 to 28.6%, and primarily from 6 to 17%. Based on the relationship between the argillaceous content and AOF (Fig. 10c), the AOF presented an apparent downward trend with increasing argillaceous content. The AOF of the Upper Shihezi, Lower Shihezi, and Taiyuan formations decreased markedly with increased argillaceous content, while the AOF of the Shanxi Formation decreased slightly, and the AOF of Shiqianfeng Formation did not show a significant change.

Thickness of gas-producing sandstone The thickness of the gas-producing sandstone had no clear effect on the AOF. The thicknesses of gas-producing sandstone ranged from 2.8 to 22.3 m, and the major part was 4−11 m. According to the relationship between the sandstone thickness and the AOF (Fig. 10d), AOF did not show an overall increasing trend as the thickness of the sandstone increased. Only the AOF of the Shiqianfeng Formation increased slightly with increasing sandstone thickness.

Controlling effects of source rock conditions

Overview of source rock conditions The gas source of the TSG in the LGF was coal-measure source rocks of the Benxi and Taiyuan formations, as well as the Shan2 Member of the Shanxi Formation. The lithology was mainly coal seams and dark mudstone, with some carbonaceous mudstone. Coal seams and dark mudstone were identified based on the core and logging response of different lithologies. The thickness of single-well coal seams ranged from 2.76 to 31.01 m, with an average of 18.8 m ($N=97$), and 84.5% coal seam thickness was 10–25 m (Fig. 11a). The w(TOC) value ranged from 27.09 to 78.18%, averaging 53.8% ($N=29$), and w(TOC) values of 50–70% accounted for 51.7% of the total (Fig. 11b). The range of S_1+S_2 was 2.35–290.8 mg/g, with an average of 87.78 mg/g ($N=25$). The thickness of the mudstone was 16.83–119.94 m, with an average of 58.8 m ($N=97$), and 70.1% of mudstone was 40–70 m thick (Fig. 11c). The w(TOC) value ranged from 0.086 to 16.91%, with an average of 4.43% ($N=40$), and the distribution was relatively balanced (Fig. 11d). The mudstone S_1+S_2 ranged from 0.11 to 18.78 mg/g, with an average of 3.42 mg/g ($N=38$).

According to the cross-plot of hydrogen index *(HI)* and pyrolysis peak temperature *(T_{max})* (Fig. 12a), the type of organic matter in the source rocks were mainly type III kerogen, followed by type II_2 kerogen, type II_1; and type I kerogen, which occurred sporadically. According to the statistics of thermal evolution degree, R_o ranged from 0.83 to 4.89%, with an average of 1.26% ($N=70$), and values of 1.0–1.3% accounted for 58.8% of the total. This indicates that the source rocks are mature and that some also have abnormally high R_o values (Fig. 12), such as the 3.19 and 4.89% for wells B1 and B2, respectively (Fig. 3). The T_{max} of the source rocks ranged from 423.8 to 551 ℃, with an average of 474.6 ℃ ($N=57$). It should be noted that the T_{max} of some wells exceeded 500 ℃ (Fig. 12b). For example, the T_{max} of wells B1, B2, and B3 were 532.8, 540.5, and 538.3 ℃, respectively (Fig. 3). These anomalous high T_{max} and R_o values may be related to the tectonic activities of the Zijinshan Structural Belt. In the Late Jurassic–Early Cretaceous (140 ~ 100 Ma), multiple stages of magmatic intrusion occurred in the Zijinshan Structural Belt (Fu et al. 2016; Zou et al. 2016; Ge et al. 2018; Du et al. 2021), with a magma cooling rate as high as 52 ℃/Ma (Ge et al. 2018). This rapid heat dissipation warmed the surrounding rock via heat conduction, resulting in the higher formation temperature adjacent to the Zijinshan rocks and the abnormal thermal evolution of the local source rock.

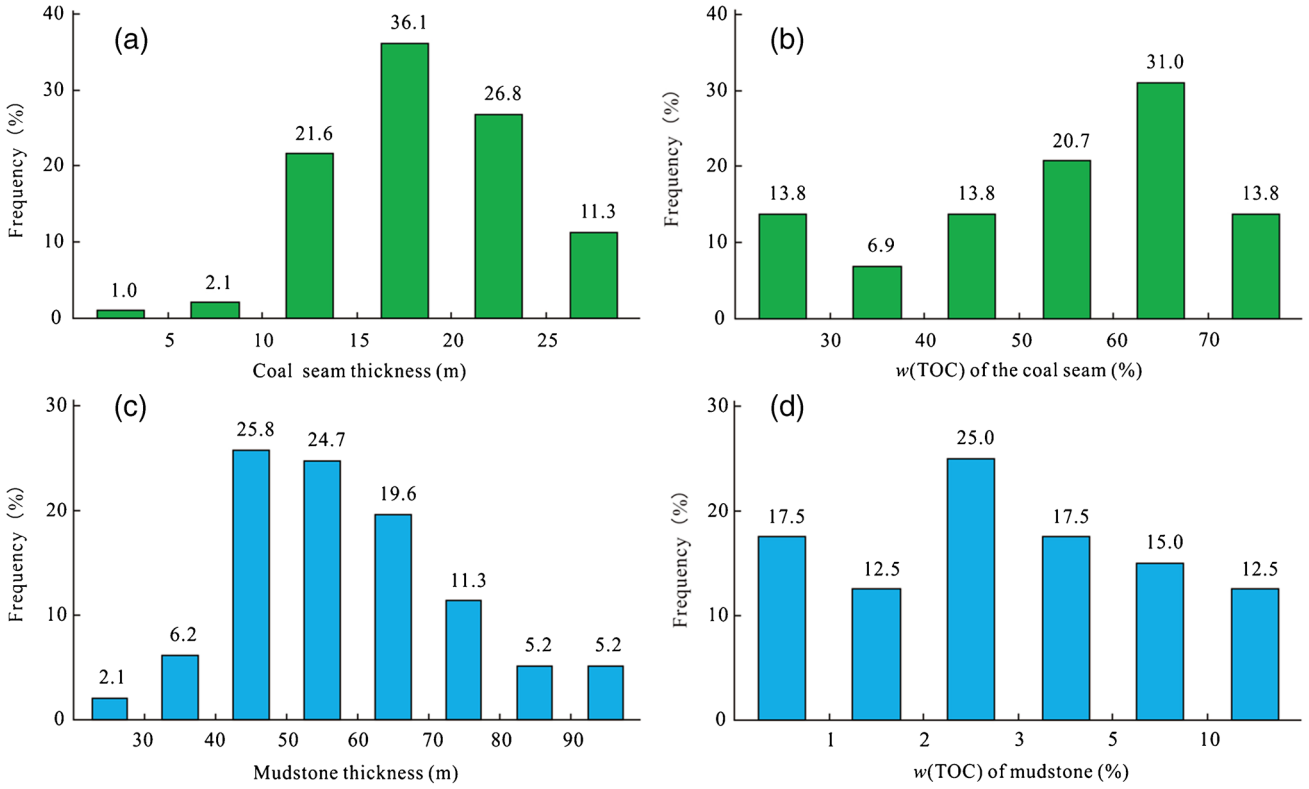

Fig. 11 Distribution histogram of different parameters of the coal-measure source rocks in the LGF. (**a**) Coal seam thickness. (**b**) Coal seam total organic carbon. (**c**) Dark mudstone thickness. (**d**) Dark mudstone total organic carbon

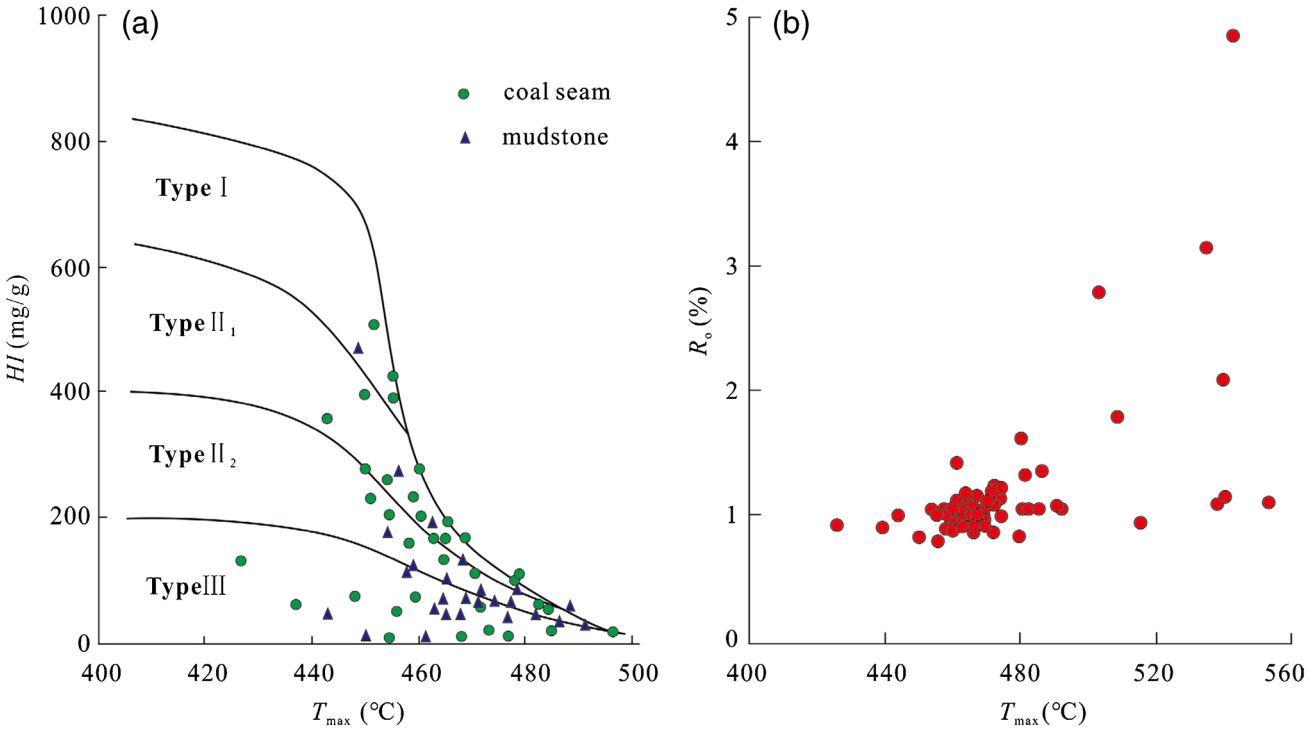

Fig. 12 Cross-plots of HI vs. T_{max} and R_o vs. T_{max} of Upper Paleozoic source rocks from the Linxing block, Ordos Basin. Note: HI is hydrogen index, T_{max} is pyrolysis peak temperature, and R_o is vitrinite reflectance

Controlling effect of source rock conditions From the relationship between coal seam thickness and AOF (Fig. 13), with an increase in coal seam thickness, AOF did not show an obvious positive or negative correlation trend. The AOF of the Upper Shihezi, Lower Shihezi, Taiyuan, and Shanxi formations did not change significantly, and only the Shiqianfeng Formation had a slightly decreasing trend. Note that the interpretation of the Benxi Formation data points

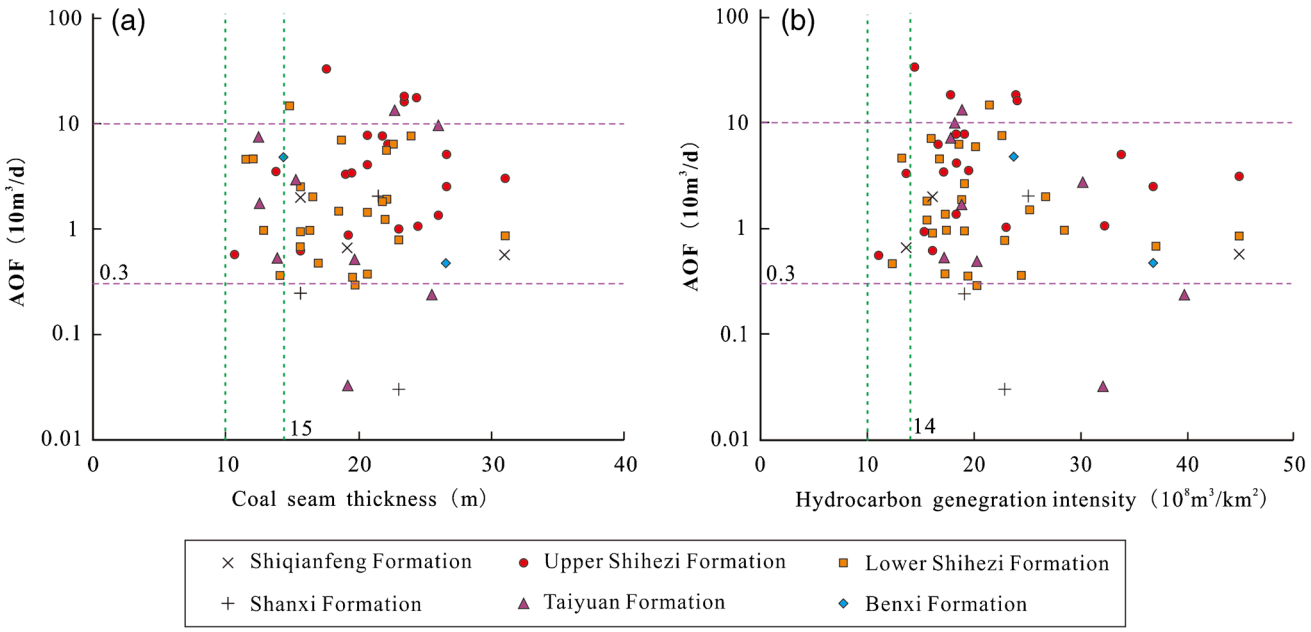

Fig. 13 Cross-plot of different parameters of coal-measure source rocks and absolute open flow (AOF) in the LGF. (**a**) Coal seam thickness vs. AOF. (**b**) Hydrocarbon generation intensity vs. AOF

was limited. Based on Eq. (1), the range of HGI for the coal-measure source rocks was (10.2–44.8)×10^8 m^3/km^2, with an average of 21.4×10^8 m^3/km^2. In terms of the relationship between HGI and AOF, AOF presented with an insignificant change trend HGI increased. In a single formation, with an increase in HGI, the Taiyuan Formation had a certain downward trend, but the changes were not obvious in the other formations except for Benxi Formation. However, when the thickness of the coal seam was greater than 10 m, or when HGI was greater than 10×10^8 m^3/km^2, the vast majority of AOF exceeded 0.3×10^4 m^3/d, i.e., the condition of commercial gas flow can be met. Moreover, when the thickness of the coal seam was greater than 15 m, or when the HGI was greater than 14×10^8 m^3/km^2, the AOF could reach 10×10^4 m^3/d. These results indicate that neither the thickness of the coal seam nor the HGI had obvious controlling effects on the degree of gas enrichment; however, the conditions of the coal-measure source rocks still provide sufficient natural gas for the formation of a multi-layer TSG reservoir.

Controlling effects of current tectonic and fault distribution

Current tectonic conditions The current structure does not control AOF; instead, it controls He8 and Tai2 members to a certain extent. As can be seen from the relationship between the current structural height and AOF (Fig. 14), as the structural height decreases, AOF generally first increases, and then decreased. The AOF of the Qian4 and Qian5 members showed a slightly increasing trend, and the AOF of the He4, He6, and He7 members showed a slightly increasing trend, while the AOF of the He2 Member showed no obvious trend. The AOF of the He8 and Tai2 members decreased as the tectonic altitude decreased. These results indicate that the AOF of He8 and Tai2 members may be influenced by local high points of tectonic altitude.

Fault conditions The fault system in the LGF was controlled by regional stress in the eastern area of the Ordos Basin. Moreover, the uplift of the Zijinshan rock mass (Wang et al. 2010; Ge et al. 2018) can be divided into two types. The first type is reverse faults controlled by regional stress, which is mostly present in the NNE−SSW and N−S directions, with high angle faults of small vertical distance, extending from the Benxi Formation to the Shiqianfeng Formation, and even into the Mesozoic sequences (Li et al. 2019b). The second type stems from the small-scale radial and arc faults developed around the Zijinshan Structural Belt, which is controlled by the upper arch of the Zijinshan rock mass. The network fault system formed by these two fault types and their associated fractures decreased in density outward from the north and west of the Zijinshan structural belt (Fig. 3), providing vertical migration channels for the formation of multi-layer TSG reservoirs.

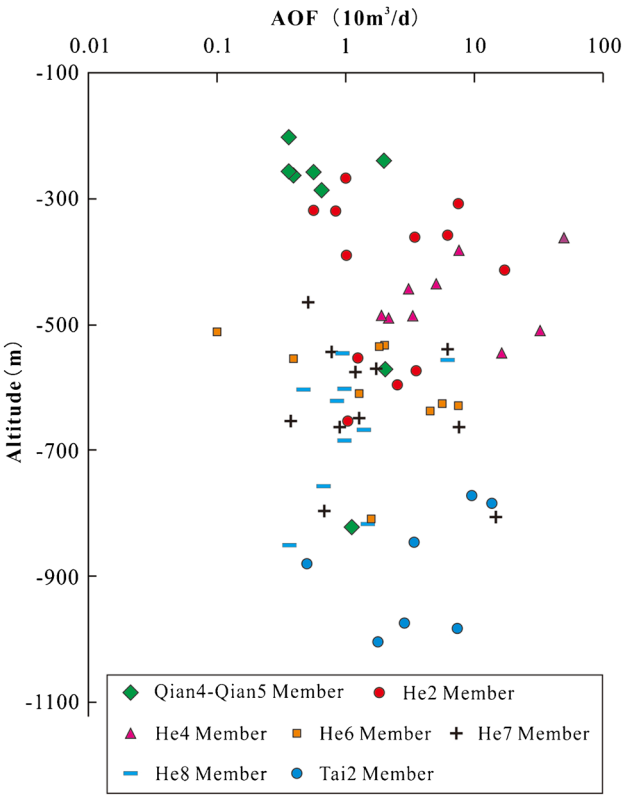

Fig. 14 Cross-plot of current tectonic altitude and AOF in the LGF

The moderately developed fault system is conducive to the formation of an effective transport system for natural gas accumulation, while the over-developed fault system facilitates the formation of natural gas escape channels. The moderate fault system in the LGF was formed by regional stress, which is more conducive to the formation of gas reservoirs. For example, according to the reservoir profile of the Upper Shihezi and Lower Shihezi formations from wells H1–H7 (Fig. 8), the fault system connected multiple layers of tight sandstone with coal-measure source rocks and served as an efficient channel for layers with an AOF higher than 5×10^4 m^3/d. These include the He6 and He7 members of Well H3, the He2 and He4 members of Well G3, and the He3 Member of Well H2. In contrast, the over-developed fault system around the Zijinshan Structural Belt cuts sandstone and mudstone, undermining the effectiveness of the sandstone traps, and extending upward to the overlying Mesozoic sequences, or even to the surface (Ge et al. 2018). This type of fault system is not conducive to the formation of TSG reservoirs in the Upper Paleozoic but may form shallow gas reservoirs or dissipate gas to the surface. At present, no gas reservoirs have been discovered near the Zijinshan Structural Belt (Fig. 3). The distance from the fault to the well ranged from 0 to 6 km, with most 0.5 to 3 km away. According to the relationship between the fault–well distance and the

AOF (Fig. 15), as the fault–well distance increases, the AOF of the upper and lower Shihezi formations (outside source rocks) showed an obvious decreasing trend, while the AOF of Shiqianfeng Formation had a decreasing trend to a certain extent, and the changing trend of the Taiyuan Formation was not obvious. These results showed that the distribution of faults had a certain control effect on the formation of gas reservoirs outside the source, i.e., the closer the distance between the faults and wells, the more favorable formation of high-yield gas reservoirs.

Natural gas enrichment model

The multi-layer tight sandstone produced gas in the LGF with a quasi-continuous distribution, which is characterized by high-quality reservoir enrichment, sufficient gas supply, moderate fault system efficiency, and a favorable local high point. The results show that the yields, from the Taiyuan Formation inside the source to the Shiqianfeng Formation outside the source, are affected by reservoir porosity, permeability, and argillaceous content, with the effect of permeability being the most obvious. In addition, the coal-measure source rocks with high TOC and medium R_o provide sufficient gas source conditions, and their HGI exceeded the formation boundary of the large gas fields (Zhao et al. 2012; Dai et al. 2014). These gas sources can be charged to multiple formations, with AOF reaching commercial gas flows. Considering the two different fault systems, the intermediate fault system provided efficient transport for vertical migration, especially to off-source gas reservoirs. The fault system developed around the Zijinshan Structural Belt was more favorable for gas migration or escape to shallow strata, and not favorable for the formation of the TSG reservoir in the upper Paleozoic. The local structural high point is the favorable position for natural gas accumulation, which is manifested in Tai2 and He8 members. Based on these results, the LGF exhibited three gas enrichment models within three areas of the gas field: X, Y, and Z, respectively (as shown previously in Fig. 3). The enrichment models are described as follows.

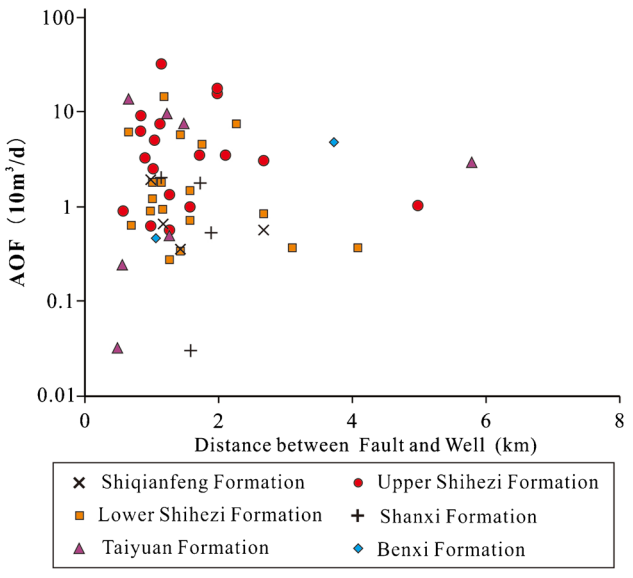

Fig. 15 Cross-plot of the distance from fault to well and AOF in the LGF

(1) X area: Excellent reservoir, highly efficient fault system, near-source gas-rich model.

This model represents the X area (Fig. 3) and virtual well M1 (Fig. 16) with characteristics of sufficient source rock conditions, excellent reservoir physical properties, a moderately developed fault system, and gas-rich accumulation that is near the source (He7 Member and above). The gas-producing layers are mainly concentrated in the He2, He3, He4, He6, and He7 members, with an average AOF of over 6×10^4 m^3/d. The model has the following favorable reservoir forming conditions: (i) The source rock conditions are sufficient. The *w*(TOC) of the coal seam ranges from 44.5 to 71.35%, with an average of 59.52%, and R_o ranges from 1.05 to 1.26%, with an average of 1.13%. The HGI is $(13.6–24)\times10^8$ m^3/km^2, with an average of 16.9×10^8 m^3/km^2. (ii) The reservoir conditions are excellent. The porosity ranges from 2.1 to 19.2% ($N=538$), with an average of 9.34%. The permeability ranges from $(0.01\text{ to }50.2)\times10^{-3}$ μm^2, with an average of 1.88×10^{-3} μm^2 and a median of 0.52×10^{-3} μm^2. The argillaceous content is low, around 15.3% ($N=46$). (iii) The density of faults developed under regional stress is moderate, connecting the coal-measure source rocks to tight sandstone traps and migrating the gas to the trap (outside source rocks, but only by a small distance), forming several TSG reservoirs along the fault system.

(2) Y area: Excellent reservoir, favorable high point, in- and adjacent-source gas-rich model.

This model represents the Y area (Fig. 3) and virtual well M2 (Fig. 16) with characteristics of sufficient source rock conditions, excellent reservoir physical properties, a favorable local high point, gas-rich accumulation of in-source (Tai2 Member), and adjacent-source (He 8 Member) formations. The main gas reservoirs are concentrated in the Tai2 and He8 members, and the maximum AOF can reach 13.3×10^4 m^3/d. The favorable conditions are as follows: (i) The source rock conditions are sufficient. The *w*(TOC) of the coal seams ranges from 44.5 to 71.35%, with an average of 59.52%, and R_o between 0.94 and 1.38%, with an average of

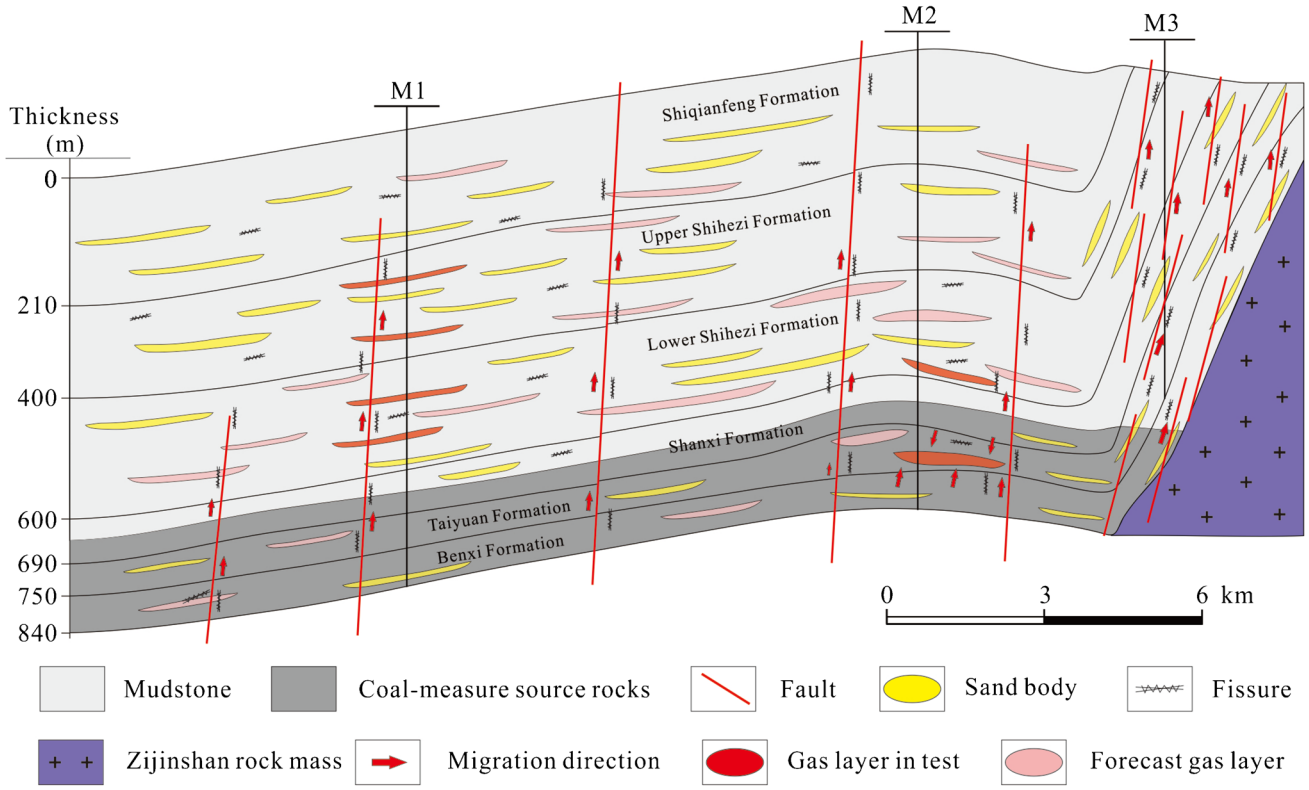

Fig. 16 Enrichment models of multi-layer tight sandstone gas in the LGF, eastern Ordos Basin, Northern China

1.18%. The HGI ranges from (15.6 to 33.9) × 10^8 m^3/km^2, with an average of 20.2 × 10^8 m^3/km^2. (ii) The reservoir conditions are extremely good. The porosity is between 0.6 and 14.1% (N = 429), with an average of 9.03%. The permeability ranges from (0.011 to 12.66) × 10^{-3} μm^2, with an average of 1.06 × 10^{-3} μm^2 and a median of 0.62 × 10^{-3} μm^2. The argillaceous content of sandstone is ~ 19% (N = 32). (iii) The tectonic high point of the thick sand body is the favorable position for gas migration, and the gas enrichment degree is relatively high.

(3) Z area: Middle reservoir, over-developed fault system, in- and out-source gas-poor model.

This model has the characteristics of excellent source rock conditions, moderately good reservoir physical properties, an over-developed fault system, gas-poor distribution of in- and out-source in the Upper Paleozoic sequences, is represented by the Z area (Fig. 3) along the Zijinshan Structural Belt and marked by the virtual well M3 (Fig. 16). To date, no natural gas reservoirs have been identified in the Upper Paleozoic sequence of this area. The model has the following conditions: (i) The source rock conditions are sufficient. The R_o of the source rock is 1.32%, which is better than in some other areas. (ii) The reservoir conditions are moderately good. The porosity ranges from 1.4 to 16.1% (N = 245), with an average of 6.71%, and the permeability is between (0.14 and 8.41) × 10^{-3} μm^2, with an average of 0.42 × 10^{-3} μm^2 and a median of 0.22 × 10^{-3} μm^2. (iii) Because of the uplift of the Zijinshan rock mass, the overlapping and interlacing fault system with high angle and excessive development cut through the sandstone reservoir and mudstone cap, leading to the upward migration of natural gas to the shallow layer and ultimately surface leakage.

Conclusion

Although the main controlling factors and enrichment model of TSG have long been a focus of research, limited attention has been paid to the multi-layer TSG reservoirs, which comprise a considerable component of unconventional natural gas exploration targets. In this study, the distribution and characteristics of the multi-layer TSG reservoirs in the LGF of the Ordos Basin in China were defined. In addition, the main controlling factors of natural gas accumulation in the reservoir were discussed, and the natural gas enrichment modes of different areas of the gas field were established. To achieve this, seismic, drilling, logging, gas testing, laboratory, and other accumulated

data were comprehensively analyzed using interpretive geo-analytical techniques. Three main findings can be summarized as follows:

(1) There are 14 sets of gas-producing layers in the Upper Paleozoic strata of the LGF, of which, the Tai2, He8, He7, He6, He4, and He2 members are the chief layers. The porosity of the gas reservoir ranged from 7 to 13%, with an average of 10.11%, and the permeability ranged from $(0.5 \text{ to } 7)\times10^{-3}$ μm^2, with a median of 0.81×10^{-3} μm^2. The tight sandstone gas reservoir comprises two sub-types: a lenticular lithological reservoir and a lithological-fault reservoir, showing quasi-continuous distribution with characteristics of being vertically superimposed and laterally continuous.
(2) The accumulation of multi-layer TSG is controlled by reservoir properties, gas source, fault system, and structural high points, and has the laws of "high-quality reservoir enrichment, sufficient gas source supply, moderate fault efficiency, and a favorable local high point."
(3) Gas enrichment models were categorized into three types and corresponding areas: (i) An X-area: Excellent reservoir, highly efficient fault system, near-source gas-rich model; (ii) Y area: Excellent reservoir, favorable high point, in- and adjacent-source gas-rich model; and (iii) the Z area: Moderately good reservoir, over-developed fault system, in- and out-source gas-poor model, distributed around the Zijinshan Structural Belt.

The findings of this study provide novel insight into the accumulation theory of TSG, as well as provide theoretical guidance for the discovery of multi-layer gas fields in the LGF and similar basins worldwide.

Acknowledgements The authors are also thankful to the reviewers of this manuscript for their constructive comments and suggestions.

Author contribution WW: methodology, writing—original draft, writing—review and editing, software. JZ: conceptualization, supervision, methodology. YW: supervision, validation, conception. MG: investigation, data statistics. HW: formal analysis, data statistics. JL: methodology. JD: data statistics and figures.

Funding This study was jointly funded by the National Science and Technology Major Project of China (grant number 2016ZX05066), the "13th Five-Year plan" Major Project of the China National Offshore Oil Corporation Limited (grant number CNOOC-KJ 135 ZDXM14 LTD), the Natural Science Foundation of Shaanxi Province (project number 2020JQ-767), and the Scientific Research Program of the Shaanxi Provincial Education Department (Program number 20JS128).

Declarations

Conflict of interest The authors declare no competing interests.

References

Bou-Hamdan KF, Abbas, AH (2021) Utilizing ultrasonic waves in the investigation of contact stresses, areas, and embedment of spheres in manufactured materials replicating proppants and brittle rocks. Arab J Sci Eng. https://doi.org/10.1007/s13369-021-06409-6

Chen G, Ding C, Xu LM, Zhang HR, Hu YX, Yang F, Li N, Mao XN (2012) Analysis on the thermal history and uplift process of Zijinshan intrusive complex in the eastern Ordos Basin. Chinese J Geophysics 55(11):3731–3741 (in Chinese). https://doi.org/10.6038/j.issn.0001-5733.2012.11.020

Chen HD, Jiang B, Qu ZH, Wang JL, Wang LL (2014) Diversity structural characteristics and control action on coal bed gas content in Linfen and Baode area. J China Coal Society 39(3):510–517 (in Chinese). DOI: https://doi.org/10.13225/j.cnki.jccs.2013.1574

Chen RY, Luo XR, Chen ZK, Yu J, Yang Y (2006) Restoration of burial history of four periods in Ordos Basin. Acta Pet Sin 27(2):43–47 (**(in Chinese)**)

Chen XZ, Pang XQ, Shao XH, Jiang FJ, Liu TS, Li LL, Zheng DY, Huyang YY (2018) Accumulation conditions of tight sandstone gas in the lower Shihezi formation in Linxing A area, Ordos Basin. Geo Sci Tech Inform 37(1):169–176 (in Chinese). https://doi.org/10.19509/j.cnki.dzkq.2018.0123

Dai JX, Qin SX, Hu GY, Ni YY, Gan LD, Huang SP, Hong F (2019) Major progress in the natural gas exploration and development in since 1947 in China. Pet Explor Dev 45(6):1–10. https://doi.org/10.1016/S1876-3804(19)60266-1

Dai JX, Ni YY, Huang SP, Liao FR, Yu C, Gong DY, Wu W (2014) Significant function of coal-derived gas study for natural gas industry development in China. Nat Gas Geosci 25(1):1–22 (in Chinese). https://doi.org/10.11764/j.issn.1672-1926.2014.01.0001

Du J, Zhu GH, Wu LF, Zhang ZH, Gao JX, Yu YJ, Ma ZJ, Zhang M (2021) "Multi-series and quasi-continuous" tight gas accumulation pattern and giant gas field exploration practice in Linxing area. Nat Gas Ind B 41(3):58–71. https://doi.org/10.3787/j.issn.1000-0976.2021.03.007

Feng FP, Huang R, Guo BY, Ai C, Hu CY, Yang L (2019) A new method for evaluating the effectiveness of hydraulic fracturing in tight reservoirs. Arab J Geosci 12:373. https://doi.org/10.1007/s12517-019-4501-2

Fu JH, Wei XS, Ren JF (2008) Distribution and genesis of large-scale Upper Palaeozoic lithologic gas reservoirs on YiShaan slope. Pet Explor Dev 35(6):664–667

Fu N, Yang SC, He Q, Xu H, Lin Q (2016) High-efficiency reservoir formation conditions of tight sandstone gas in Linxing-Shenfu blocks on the east margin of Ordos Basin. Acta Pet Sin 37(S1):111–120 (in Chinese). DOI:https://doi.org/10.7623/syxb2016S1011

Gao DC, Guo C, Jiang CF, Zhang LX, Wang H, Shi P, Chen YY (2018) Hydrocarbon generation simulation of low-maturity shale in Shanxi Formation, Ordos Basin. Pet Geol & Exp 40(3):454–460 (In Chinese). https://doi.org/10.11781/sysydz201803454

Ge Y, Zhu GH, Wan H, Pan XZ, Huang ZL (2018) The influence of Zijinshan structural belt to the formation and distribution of tight sandstone gas reservoir in Upper Paleozoic, in the eastern Ordos Basin. Nat Gas Geosci 29(4):491–499 (in Chinese). https://doi.org/10.11764/j.issn.1672-1926.2018.03.008

He JC, Yu HJ, He GH, Zhang J, Li Y (2021) Natural gas development prospect in Changqing gas province of the Ordos Basin. Nat Gas Ind B 41(8):23–33. https://doi.org/10.1016/j.ngib.2021.08.023

Hu WQ, Li YB, Chen X, Ma LT, Liu C, Huang Y, Qiao F, Wang D, Liu ZZ (2020) Origin and source of natural gas in the Upper Paleozoic in Linxing area, Ordos Basin. Nat Gas Geosci 31(1):26–36 (in Chinese). https://doi.org/10.11764/j.issn.1672-1926.2019.08.009

Huang JJ (1991) Petrology and petrogenesis of Zijinshan alkaline ring complex from Linxian County, Shanxi Province, China. Mod Geosci 5(1):24–29 ((**in Chinese**))

Huang SP, Fang X, Liu D, Fang CC, Huang TF (2015) Natural gas genesis and sources in the Zizhou gas field, Ordos Basin, China. Int J Coal Geol 152:132–143. https://doi.org/10.1016/j.coal.2015.10.005

Jiu B, Huang WH, Li Y, He MQ (2021) Influence of clay minerals and cementation on pore throat of tight sandstone gas reservoir in the eastern Ordos Basin, China. J Nat Gas Sci Eng 87:103762. https://doi.org/10.1016/j.jngse.2020.103762

Kong XX, Xiao DS, Jiang S, Lu SF, Sun B, Wang JM (2020) Application of the combination of high-pressure mercury injection and nuclear magnetic resonance to the classification and evaluation of tight sandstone reservoirs: a case study of the Linxing Block in the Ordos Basin. Nat Gas Ind B 40(3):38–47. https://doi.org/10.1016/j.ngib.2020.09.001

Li GZ, Qin Y, Jian S, Wu P, Li C, Wei KH, Zhu C (2019a) Geochemical characteristics of tight sandstone gas and hydrocarbon charging history of Linxing area in Ordos Basin, China. J Petro Sci Eng 177:198–207. https://doi.org/10.1016/j.petrol.2019.02.023

Li LT, Wu KQ, Liang JH, Chen GH, Zhang L, Guo GS (2019b) The domination of tight sand gas accumulation by the Zijinshan thermal event in the block B, eastern Ordos Basin. Nat Gas Geosci 30(10):1430–1438 (in Chinese). https://doi.org/10.11764/j.issn.1672-1926.2019b.08.009

Li WH, Zhang Q, Li KY, Chen Q, Guo YQ, Ma Y, Feng JP, Zhang DF (2021) Sedimentary evolution of the late Paleozoic in Ordos Basin and its adjacent areas. J Palaeogeo 23(1):39–53 (in Chinese). https://doi.org/10.7605/gdlxb.2021.01.003

Li Y, Tang D, Elsworth D, Xu H (2014) Characterization of coalbed methane reservoirs at multiple length scales, a cross-section from southeastern Ordos Basin, China. Energy Fuels 28:5587–5595. https://doi.org/10.1021/ef500449s

Li Y, Tang DZ, Wu P, Niu XL, Wang K, Qiao P, Wang ZS (2016) Continuous unconventional natural gas accumulations of Carboniferous-Permian coal-bearing strata in the Linxing area, northeastern Ordos basin, China. J Nat Gas Sci Eng 35:314–327. https://doi.org/10.1016/j.jngse.2016.10.037

Mi LJ, Zhu GH (2021) Geological characteristics and exploration breakthrough in Linxing-Shenfu tight gas field, northeastern Ordos Basin. China Petro Explor 26(3):53–67 ((**in Chinese**))

Shen J, Li KX, Zhang HW, Shabbiri K, Hu QJ, Zhang C (2021) The geochemical characteristics, origin, migration and accumulation modes of deep coal-measure gas in the west of Linxing block at the eastern margin of Ordos Basin. J Nat Gas Sci Eng 91:103965. https://doi.org/10.1016/j.jngse.2021.103965

Shu Y, LinYX LY, Yu ZY (2019) Control of magmatism on gas accumulation in Linxing area, Ordos Basin, NW China: Evidence from fluid inclusions. J Pet Sci Eng 180:1077–1087. https://doi.org/10.1016/j.petrol.2019.06.034

Shu Y, Sang SX, Lin YX, Zhou XZ, Wang H, Wang ZL (2021) The influence of magmatic-hydrothermal activities on porosity and permeability of sandstone reservoirs in the Linxing area, Ordos Basin, Northern China. J Asian Earth Sci 213:104741. https://doi.org/10.1016/j.jseaes.2021.104741

Song P, Guo MQ, Zhao JJ, Li J (2019) Characteristics of Upper Paleozoic source rocks in Linxing area, eastern margin of Ordos Basin and their controlling effect on accumulation of natural gas. J Xi'an Shiyou Univ 34(1):22–28 (in Chinese). https://doi.org/10.3969/j.issn.1673-064X.2019.01.003

Sun LD, Zou CN, Jia AL, Wei YS, Zhu RK, Wu ST, Guo Z (2019) Development characteristics and orientation of tight oil and gas in China. Pet Explor Dev 46(6):1015–1026. https://doi.org/10.11698/PED.2019.06.01

Tang X, Zhang JC, Shan YS, Xiong JY (2012) Upper Paleozoic coal measures and unconventional natural gas systems of the Ordos Basin, China. Geosci Front 3(6):863–873. https://doi.org/10.1016/j.gsf.2011.11.018

Wang XY, Zhang QL, Wang LS, Ge RF, Chen J (2010) Structural features and tectonic stress fields of the Mesozoic and Cenozoic in the eastern margin of the Ordos basin, China. Geo Bull China 29(8):1168–1176 ((**in Chinese**))

Wang T, Xu MJ, Wang LS, Liu SW, Hu XZ (2007) Aeromagnetic anomaly analysis of Ordos and adjacent regions and its tectonic implications. Chinese J Geophysics 50(1):163–170 ((**in Chinese**))

Wu HY, Guo MQ, Zhao JZ, Li J, Wu WT, Chen YH, Song P (2021a) Densification mechanisms of tight sandstones in closed to semi-closed systems: typical example from the Upper Paleozoic in the Linxing area, Ordos Basin. Arab J Geosci 14:1167. https://doi.org/10.1007/s12517-021-07535-z

Wu WT, Chen MN, Li N, Wang Y, Zhao JZ, Wei XS (2021b) Characteristics of coal-measure source rock and its controlling effect on gas-water distribution of tight sandstone of He8 Member in Sulige Gas Province, Ordos Basin. Energy Explor Exploit 39(5):1727–1746. https://doi.org/10.1177/01445987211022440

Wu WT, Zhao JZ, Wei XS, Wang Y, Zhang J, Wu HY, Li J (2022) Evaluation of gas-rich "sweet-spot" and controlling factors of gas–water distribution in tight sandstone gas provinces: an example from the Permian He8 Member in Sulige Gas Province, central Ordos Basin, Northern China. J Asian Earth Sci 227:105098. https://doi.org/10.1016/j.jseaes.2022.105098

Xie YG, Qin Y, Ye JP, Pan XZ, Gao LJ, Duan CJ (2016) Accumulation conditions of tight gas in the Upper Paleozoic of Linxing Block. J China Coal Society 41(1):181–191(in Chinese). https://doi.org/10.13225/j.cnki.jccs.2015.9010

Xue CQ, Zhong JH, Hou MX, Li FT, Peng CF (2019) Sedimentary facies distribution and the characteristics of transitional shale in the upper Palaeozoic in northeast Ordos basin, China. Arab J Geosci 12(16):1–10. https://doi.org/10.1007/s12517-019-4669-5

Yang H, Fu JH, Liu XS, Meng PL (2012) Accumulation conditions and exploration and development of tight gas in the Upper Paleozoic of the Ordos Basin. Pet Explor Dev 39(3):295–303

Yang H, Fu JH, Wei XS, Liu XS (2008) Sulige field in the Ordos Basin: geological setting, field discovery and tight gas reservoirs. Mar Pet Geol 25:387–400. https://doi.org/10.1016/j.marpetgeo.2008.01.007

Yang H, Wei XS (2007) New progress achieved by natural gas exploration in Sulige area. Nat Gas Ind 27(12):6–11 ((**in Chinese**))

Yang H, Xi SL, Wei XS, Chen YC (2016) Accumulation theories of large tight sandstone gas of Ordos Basin. Science Press, Beijing ((**in Chinese**))

Yin XD, Jiang S, Li YL, Gao W, Lu JG, Wu P, Ma LT (2020) Impact of pore structure and clay content on the water-gas relative permeability curve within tight sandstone: a case study from the LS block, eastern Ordos Basin, China. J Nat Gas Sci Eng 81:103418. https://doi.org/10.1016/j.jngse.2020.103418

Zhao JZ, Fu JH, Yao JL, Wang HE, Cao Q, Wang XM, Ma YP, Fan YF (2012) Quasi-continuous accumulation model of large tight sandstone gas field in ordos basin. Acta Pet Sin 33(S1):37–52 ((**in Chinese**))

Zhao JZ, Fu JH, Cao Q, Wang DX, Bai YB, Li J, Meng QA, Er C, Wu WT, Liu ZD, Wang YG, Wang XM, Si SH, Xu ZY, Pang CX (2017) Tight oil and gas accumulation theory and evalution technology Petro. Ind. Press:131–145

Zhao JZ, Li J, Cao Q, Bai YB, Wu WT, Ma YP (2019) Quasi-continuous hydrocarbon accumulation: an alternative model for the formation of large tight oil and gas accumulations. J Pet Sci Eng 174:25–39. https://doi.org/10.1016/j.petrol.2018.10.076

Zheng DY, Pang XQ, Jiang FJ, Liu TS, Shao XH, Huyan YY (2020) Characteristics and controlling factors of tight sandstone gas

reservoirs in the Upper Paleozoic strata of Linxing area in the Ordos Basin. China J Nat Gas Sci Eng 75:103135. https://doi.org/10.1016/j.jngse.2019.103135

Zou CN, Qiu Z (2021) Preface: New advances in unconventional petroleum sedimentology in China. Acta Sedimentol. Sin. 39(1):1–8 (in Chinese). https://doi.org/10.14027/j.issn.1000-0550.2021.001

Zou W, Chen HQ, Yang B, He BW, Gui ZH, Shang H (2016) Zijinshan pluton characteristics in Linxian,Shanxi,China,and its function of tight gas accumulation. Geophys Prosp Pet 51(S1):120–125 (in Chinese). DOI: https://doi.org/10.13810/j.cnki.issn.1000-7210.2016.s.020